Biogeosciences Discuss., 11, 8259–8324, 2014
www.biogeosciences-discuss.net/11/8259/2014/
doi:10.5194/bgd-11-8259-2014

Biogeosciences Discussions
Open Access

Pigments, elemental composition (C, N, P, Si) and stoichiometry of particulate matter, in the naturally iron fertilized region of Kerguelen in the Southern Ocean

M. Lasbleiz[1], K. Leblanc[1], S. Blain[2], J. Ras[3,4], V. Cornet-Barthaux[1], S. Hélias Nunige[1], and B. Quéguiner[1]

[1]Aix-Marseille Université Université de Toulon, CNRS/INSU, IRD, MIO, UM 110, 13288, Marseille, Cedex 09, France
[2]Laboratoire d'Océanographie Microbienne (LOMIC), UMR7621, CNRS, Université Pierre et Marie Curie, 66650, Banyuls-sur-mer, France
[3]Laboratoire d'Océanographie de Villefranche, UMR7093, CNRS, 06230 Villefranche-sur-Mer, France
[4]Université Pierre et Marie Curie (Paris-6), Unité Mixte de Recherche 7093, Laboratoire d'Océanographie de Villefranche-sur-Mer, 06230, Villefranche-sur-Mer, France

Received: 20 May 2014 – Accepted: 20 May 2014 – Published: 5 June 2014

Correspondence to: M. Lasbleiz (marine.lasbleiz@univ-amu.fr)

Published by Copernicus Publications on behalf of the European Geosciences Union.

BGD
11, 8259–8324, 2014

Abstract

The particulate matter distribution and phytoplankton community structure of the iron-fertilized Kerguelen region were investigated in early austral spring (October–November 2011) during the KEOPS2 cruise. The iron-fertilized region was characterized by a complex mesoscale circulation resulting in a patchy distribution of particulate matter. Integrated concentrations over 200 m ranged from 72.2 to 317.7 mg m^{-2} for chlorophyll *a*, 314 to 744 mmol m^{-2} for biogenic silica (BSi), 1106 to 2268 mmol m^{-2} for particulate organic carbon, 215 to 436 mmol m^{-2} for particulate organic nitrogen, and 29.3 to 39.0 mmol m^{-2} for particulate organic phosphorus. Three distinct high biomass areas were identified: the coastal waters of Kerguelen Islands, the easternmost part of the study area in the Polar Front Zone, and the southeastern Kerguelen Plateau. As expected from previous artificial and natural iron-fertilization experiments, the iron-fertilized areas were characterized by the development of large diatoms revealed by BSi size–fractionation and HPLC pigment signatures, whereas the iron-limited reference area was associated to a low biomass dominated by a mixed (nanoflagellates and diatoms) phytoplankton assemblage. A major difference from previous artificial iron fertilization studies was the observation of much higher Si : C, Si : N, and Si : P ratios (respectively 0.31 ± 0.16, 1.6 ± 0.7 and 20.5 ± 7.9) in the iron-fertilized areas compared to the iron-limited reference station (respectively 0.13, 1.1, 5.8). A second difference is the patchy response of the elemental composition of phytoplankton communities to large scale natural iron fertilization. Comparison to the previous KEOPS1 cruise also allowed to address the seasonal dynamics of phytoplankton bloom over the southeastern plateau. From POC, PON, and BSi evolutions, we showed that the elemental composition of the particulate matter also varies at the seasonal scale. This temporal evolution followed changes of the phytoplankton community structure as well as major changes in the nutrient stocks progressively leading to silicic acid exhaustion at the end of the productive season.

BGD
11, 8259–8324, 2014

Our observations suggest that the specific response of phytoplankton communities under natural iron fertilization is much more diverse than what has been regularly observed in artificial iron fertilization experiments and that the elemental composition of the bulk particulate matter reflects phytoplankton taxonomic structure rather than being a direct consequence of iron availability.

1 Introduction

Considered as the largest High Nutrient Low Chlorophyll (HNLC) region in the world, the Southern Ocean is characterized by low phytoplankton productivity despite nutrient-rich waters (Martin et al., 1991; Sarmiento et al., 2004). The "Iron Hypothesis" is now largely acknowledged to explain this paradox. Martin et al. (1990) estimated that new production could be enhanced about 30-fold under iron-replete conditions and could thus stimulate the export of carbon (C) to the deep ocean by fixing atmospheric CO_2. This hypothesis motivated several artificial iron (Fe) enrichment experiments in different HNLC areas all over the world (Boyd et al., 1999; Takeda, 1998; de Baar et al., 2005; Boyd, 2007). All these studies confirmed that addition of Fe stimulated phytoplankton growth but none clearly demonstrated an enhanced C sequestration at depth (Buesseler et al., 2004). This could result from experimental artifacts, and especially from the shorter duration of experiments compared to that of vertical export processes.

To overcome those experimental constraints, the concept of "natural fertilization laboratory" was coined by Blain et al. (2007). The objective was to investigate the response of ecosystem functioning and biogeochemical cycles in a naturally iron-fertilized system by comparison with a nearby typical HNLC environment. In the early 2000s, five projects addressed this concept in different regions of the Southern Ocean: the KErguelen Ocean and Plateau compared Study (KEOPS1) (Blain et al., 2007), the CROZet natural iron bloom and EXport experiment (CROZEX) (Pollard et al., 2009), the Blue Water Zone (BWZ) program (Zhou et al., 2010, 2013), the Discovery 2010 cruises (Tarling et al., 2012), and the Dynamic Light on Fe limitation (DynaLiFe) project (Arrigo and

BGD
11, 8259–8324, 2014

Alderkamp, 2012). Each of these studies focused on recurrent seasonal blooming regions characterized by large bathymetric discontinuities (such as ridges, islands and/or submarine plateaus) and strong hydrodynamic forcings (especially geostrophic fronts), which together interact and generate natural iron inputs to surface waters. The natural iron enrichment experiments consistently verified an enhanced efficiency of C export within the naturally Fe-fertilized systems which was approximately 3 times higher than in the surrounding Fe-limited areas (Morris and Charette, 2013). However, some gaps still persist regarding the understanding of the factors controlling the dynamics of phytoplankton blooms in naturally Fe-fertilized systems of the Southern Ocean.

Previous studies in the literature have documented the influence of iron on both the structure and the elemental ratios of phytoplankton communities. The phytoplankton community structure is known to directly impact the fate of carbon through sinking rates depending on various factors such as cell size, ballast minerals, transparent exopolymers (TEP), or (re)packaging in zooplankton fecal pellets (Margalef, 1965; Falkowski et al., 2003; Legendre and Le Fèvre, 1989; Armstrong et al., 2009). Artificial and natural iron-fertilization experiments evidenced the preferential development of large diatoms (> 20 µm) under iron-replete conditions (Hutchins and Bruland, 1998; Takeda, 1998; Hare et al., 2005; Armand et al., 2008; Timmermans et al., 2008). In a recent review paper, Quéguiner (2013) proposed a conceptual general scheme for phytoplankton development in naturally Fe-fertilized systems where phytoplankton are separated into two groups occupying different niches in the water column according to their adaptation to limiting proximal factors (iron, silicic acid, and light) and their resistance to grazing by micro- and mesozooplankton. Diatoms are responsible for more than 40 % of the global oceanic primary production (Nelson et al., 1995). Large diatoms favor the export and sequestration of carbon (Nelson et al., 1995; Buesseler, 1998). Diatom growth can be controlled by silicic acid (H_4SiO_4) availability, an essential nutrient for the formation of diatom frustules. Together Fe and H_4SiO_4 could be co-limiting (Dugdale et al., 1995) and could directly alter the stoichiometry of biogenic matter by influencing the uptake rates of major elements. Both artificial and natural iron-fertilization experiments

BGD
11, 8259–8324, 2014

reported higher Si : C, Si : N and Si : P ratios under Fe-stress compared to Fe-replete conditions (Hutchins and Bruland, 1998; Franck et al., 2000; Moore et al., 2007). Thus, Fe limitation seemed to promote the development of more heavily silicified diatoms by strongly enhancing the Si compared to C and N uptake rates (de Baar et al., 1997; Firme et al., 2003). However, some exceptions were soon documented. For example, Hutchins et al. (1998) observed that Fe could sometimes limit phytoplankton growth without changing the Si : C and Si : N ratios. The control of phytoplankton elemental ratios in response to iron availability therefore remains poorly understood, which clearly calls for new observations.

During the first KEOPS cruise (KEOPS1), conducted in January–February 2005, the impact of iron on H_4SiO_4 and nitrate (NO_3^-) utilization by diatoms was investigated in the southeastern part of the naturally iron-fertilized Kerguelen Plateau (Mosseri et al., 2008; Timmermans et al., 2008). In this area, an annual bloom of diatoms depleting dissolved inorganic carbon (DIC) in surface waters (Jouandet et al., 2008) is sustained by continuous iron inputs at the surface thanks to the enhanced vertical inputs of iron-rich deep waters from the plateau (Blain et al., 2007; Park et al., 2008a). Unexpectedly, Mosseri et al. (2008) reported moderate differences in elemental ratios (Si : C : N) of the particulate matter between Fe-fertilized waters and HNLC waters. This observation was attributed to the combined effects of the presence of an already decaying diatom bloom over the plateau, and the presence of heavily silicified diatoms in HNLC waters. H_4SiO_4 : DIC and $H_4SiO_4 : NO_3^-$ elemental uptake ratios of the natural diatom community of the plateau were close to 0.13 and 1 respectively, as expected for diatoms growing in nutrient-replete conditions (Hutchins and Bruland, 1998; Takeda, 1998). However, the high NO_3^- concentrations in surface waters compared to H_4SiO_4 depletion at the end of the bloom suggested a strong decoupling between the seasonal consumption of these two nutrients. According to Mosseri et al. (2008), this could be due to differential remineralisation between Si and N and by the capacity of diatoms to grow preferentially on ammonium, thereby preventing the complete utilization of the winter NO_3^- stock. In the context of the "silicic acid leakage hypothesis" of

BGD
11, 8259–8324, 2014

Matsumoto et al. (2002), this unexpected decoupling between H_4SiO_4 and NO_3^- consumptions, if extended over the entire Permanently Open Ocean Zone (POOZ) of the Southern Ocean, could have large implications at global scale in the control of low latitude productivity and phytoplankton assemblages (Sarmiento et al., 2004). Moreover, understanding this decoupling is of critical importance to assess the efficiency of Fe fertilization in terms of DIC uptake at regional and global scales.

In order to follow up on KEOPS1 observations, the second KEOPS cruise (KEOPS2) was conducted in the naturally iron-fertilized region of Kerguelen Plateau (KP) during austral spring (October–November) 2011. Focused east of the Kerguelen Islands (KI), the study investigated the biogeochemical cycles and phytoplankton community structures in contrasted environments differently impacted by iron availability and mesoscale activity. In this paper, we examine the particulate matter distribution in relation to the phytoplankton community structure in these contrasted environments. By combining KEOPS1 data corresponding to the late stage of the bloom, the temporal evolution of phytoplankton community over the KP will be documented during the entire blooming period. The aim is to assess the seasonal degree of coupling between C, N, P, and Si cycles to better understand the seasonal dynamics of phytoplankton blooms in naturally Fe-fertilized region. The use of lithogenic silica as a proxy for lithogenic matter is discussed to track potential sources of Fe in the KP region.

2 Method

2.1 Sampling strategy

The KEOPS2 cruise was conducted in austral spring from 10 October to 20 November 2011 aboard the R/V *Marion Dufresne* (TAAF/IPEV). This research project was focused east of the KP which is characterized by the passage of the Polar Front (PF), as illustrated in Fig. 1. The KP region is surrounded by the Antarctic Circumpolar Current (ACC) whose main branch circulates to the north of the plateau (Park et al., 2008b).

BGD
11, 8259–8324, 2014

A southern branch of the ACC circulates to the south of Kerguelen Islands to further join a branch of the Fawn Trough Current (FTC). The FTC has a main northeast direction, but a minor branch splits away northwestward to rejoin the eastern side of the KP (Park et al., 2008b). These particular hydrographic features generate contrasted environments which are differently impacted by iron availability and mesoscale activity. Among these contrasted environments, KEOPS2 focused on the northeastern Kerguelen bloom (E stations), the eastern bloom (FL and FS stations) in the Polar Front Zone (PFZ), and the southeastern KP bloom (A3 station). The latter was visited twice (A3-1 in October and A3-2 in November) at a reference station that had been already studied during the KEOPS1 cruise. For comparison, the station R was considered as representative of the HNLC off-plateau area. A temporal evolution study of the northeastern Kerguelen bloom was led on the complex recirculation system located in a stationary meander of the PF. This site (referred as stations E including E1, E2, E3, E4E and E5) was visited five times in the course of the cruise. Across this complex system, two transects were sampled to get a detailed description of the biogeochemical parameters of the eastern Kerguelen area. The first transect, oriented south to north (TNS), was sampled from 21 to 23 October; the second transect, oriented west to east (TEW), was sampled from 31 October to 2 November.

Seawater samples were collected using a Seabird *SBE 911-plus* CTD unit mounted on a 24 12 L bottles rosette. A total of 30 different stations were sampled for analysis of particulate (biogenic and lithogenic) silica, particulate organic matter (carbon, nitrogen and phosphorus) and biomarker pigments. Sampling was performed at 6 to 24 depths over the water column and covered a wide range of bottom depths from 84 m to 2786 m above and off-plateau respectively.

2.2 Biogenic and lithogenic silica stocks

For particulate silica analyses, size fractionation was perfomed by filtering 2 L seawater onto stacked 0.8 and 20 µm Nucleopore® polycarbonate filters simultaneously. Samples were folded in 4 and stored in Eppendorf vials, dried overnight at 60 °C before

BGD
11, 8259–8324, 2014

being closed and stored at room temperature. Biogenic silica (BSi) and lithogenic silica (LSi) were measured following the triple extraction procedure described by Ragueneau et al. (2005). Dried filters were digested two times at 95 °C for 45 mn with an analysis of both Si and Al concentrations at each step. In order to correct BSi for LSi contamination, particulate aluminum was measured in parallel by the Lumogallion fluorescence method of Hydes and Liss (1976) adapted by Howard et al. (1986). After the double alkaline digestion, a third extraction in 2.9 mol L^{-1} hydrofluoric acid was performed on dried filters during 48 h. Blank values were 1.0 ± 0.2 nmol L^{-1} for BSi, 16 ± 7 nmol L^{-1} for LSi and 24 ± 9 nmol L^{-1} for particulate Al. This implied detection limits, defined by the sum of the average blank value plus three times the standard deviation of the blanks, of 1.6 nmol L^{-1}, 37 nmol L^{-1} and 51 nmol L^{-1} for BSi, LSi and particulate Al respectively. For some samples, Al concentrations analyzed after the second NaOH extraction were inferior to the detection limit. These samples were also characterized by the lowest LSi concentrations. The correction of the lithogenic interference is only valid considering that Al content of diatom frustules is negligible as compared to that of LSi (Schlüter and Rickert, 1998). According to Ragueneau et al. (2005), in the case of low LSi concentrations, as in open ocean waters, the interference of diatom Al may overestimate LSi concentrations. For these reasons, we decided not to apply the Al correction for samples with Al concentrations below the quantification limit, defined by the sum of the average blank value plus ten times the standard deviation of the blanks (114 nmol L^{-1}). This concerns especially off-plateau stations far from the influence of Kerguelen Islands.

2.3 Particulate organic carbon (POC), nitrogen (PON) and phosphorus (POP)

For POC and PON measurements, 1 L seawater samples were collected. For POP measurements 0.5 L seawater samples were collected. Samples were filtered onboard on 25 mm Whatman GF/F filters (precombusted at 450 °C) and stored in precombusted glass vial. Filters were dried several days at 60 °C, then sealed with an aluminium cap and stored at room temperature. In order to remove inorganic car-

BGD
11, 8259–8324, 2014

bon, POC/PON filters were acidified with fuming HCl. Finally, POC and PON concentrations were determined using the combustion method of Strickland and Parsons (1972) on an EA 2400 CHN Analyzer. POP filters were digested following the wet oxidation method described by Pujo-Pay and Raimbault (1994). Extracts were clarified through 0.2 µm Nucleopore® polycarbonate filters before being analyzed on a 3-SEAL autoanalyzer. Blanks were $1.27 \pm 0.26\,\mu mol\,L^{-1}$ for POC, $0.06 \pm 0.02\,\mu mol\,L^{-1}$ for PON and $0.011 \pm 0.005\,\mu mol\,L^{-1}$ for POP. The detection limits, defined as above, were 2.05 and $0.12\,\mu mol\,L^{-1}$ for POC and PON and $0.026\,\mu mol\,L^{-1}$ for POP. Most samples collected below 100 m showed POC concentrations inferior to the quantification limit ($3.87\,\mu mol\,L^{-1}$). To compare integrated concentrations of particulate matter over the same depth (200 m), we decided to estimate these low POC concentrations as the minimum detectable concentration ($2.05\,\mu mol\,L^{-1}$). This approximation seems reasonable considering that PON and POP standing stocks were mostly concentrated in the upper 100 m.

2.4 Pigment measurements

For pigment analyses, seawater samples were filtered through 25 mm Whatman GF/F filters. The filtered volumes varied from 1 L to 2.2 L according to the charge in particles. Filters were then placed in cryotubes and stored in liquid nitrogen. In the laboratory, pigments were extracted and analyzed following the procedure of Van Heukelem and Thomas (2001) modified by Ras et al. (2008). Filters were extracted in 3 mL methanol (100 %) for 2 h at −20 °C. The extracts were then vacuum-filtered onto Whatman GF/F filters. Within 24 h of extraction, extracts were analyzed by High Performance Liquid Chromatography (HPLC) with a complete Agilent Technologies 1200 series system. Separation of pigments was performed by means of a reversed phase C8 Zorbax Eclipse XDB column (3 × 150 mm; 3.5 µm particle size). Concentrations were calculated from the peak area obtained by diode array detection at 450 nm for carotenoids, chlorophylls *c* and *b*, 667 nm for chlorophyll *a* and derived pigments and 770 nm for bacteriochlorophyll *a*. An internal standard correction (Vitamine E acetate, Sigma) and

BGD
11, 8259–8324, 2014

external calibration standards (provided by DHI Water and Environment in Denmark) were applied for calculations of pigment concentrations. This method enabled detection of 25 pigments with low detection limits (varying from 0.1 ng L^{-1} for chlorophyll *b* to 0.4 ng L^{-1} for chlorophyll *a* and alloxanthin, considering a filtered volume of 1 L of seawater). Following the methods of Claustre (1994) and Vidussi et al. (2001) modified by Uitz et al. (2006), seven diagnostic pigments were used as biomarkers of specific phytoplankton taxa to assess the contribution of three pigment-based size classes (micro-, nano-, and picophytoplankton) to the total phytoplankton biomass. The seven pigments are fucoxanthin (Fuco), peridinin (Peri), alloxanthin (Allo), 19′-butanoyloxyfucoxanthin (19′BF), 19′-hexanoyloxyfucoxanthin (19′HF), zeaxanthin (Zea), and total chlorophyll *b* (TChl *b*). Microphytoplankton (> 20 µm) is associated to Fuco and Peri pigments. Nanophytoplankton (2–20 µm) is associated to Allo, 19′BF and 19′HF pigments. Picophytoplankton (< 2 µm) is associated to Zea and TChl *b* pigments.

3 Results

3.1 Phytoplankton pigments: biomass and community composition

3.1.1 Spatial variability over the study area

The study area was characterized by an heterogeneous distribution of vertically integrated chlorophyll *a* concentrations (Chl *a*, in Fig. 2a). It is important to keep in mind that this overview of the study area was also influenced by the rapid temporal evolution of the phytoplankton blooms. The TNS transect and station A3-1 were sampled at the start of the bloom, ten days before sampling the TEW transect including stations FL and FS. Satellite images (d'Ovidio et al., 2012) revealed that during the TEW transect, the bloom was rapidly developing with a large spatial heterogeneity.

The lowest integrated Chl *a* concentrations were found at the off-plateau stations R (39.0 mg m^{-2}) and TNS1 (52.1 mg m^{-2}). Maximum concentrations were observed at

BGD
11, 8259–8324, 2014

TEW7 (223.0 mg m^{-2}) and FL (353.8 mg m^{-2}), evidencing a very high phytoplankton biomass in the PFZ. The Polar Front clearly isolated these very high Chl *a* waters from comparatively lower Chl *a* southern waters (ranging from 100.0 to 187.7 mg m^{-2}).

In the same way, the study area was characterized by an heterogeneous distribution of phytoplankton communities as revealed by pigment biomarkers (Fig. 2b–d). The phytoplankton community was mainly dominated by microphytoplankton (representing on average 83 % of total Chl *a* biomass) all over the study area. The microphytoplankton contribution was however clearly lower at stations R and TNS1 (47 and 39 % of total Chl *a* biomass respectively) due to a higher proportion of nanophytoplankton (39 and 41 % of total Chl *a* biomass respectively). Stations TNS1 and TNS2 also departed from this general trend by exhibiting a higher picophytoplankton contribution (~ 20 % of total Chl *a* biomass) as compared to the other stations (< 10 % of total Chl *a* biomass).

Chl *a* : Fuco ratios (2.3 ± 0.4; data not shown) were within the typical range of values (1.1 to 2.3) for diatoms (Wright and Jeffrey, 1987; Tester et al., 1995; Ediger et al., 2001) except for the off-plateau stations R and TNS1, where higher ratios (4.3 ± 0.8) were found. Fucoxanthin is the dominant biomarker for diatoms but is also found in some prymnesiophytes (e.g. *Phaeocystis* sp.), chrysophytes (e.g. silicoflagellates such as *Dictyocha* sp.) and dinoflagellates. The very low concentrations in 19′BF, 19′HF and peridinin at all stations (ranging from 0.8 to 9.7, 1.9 to 12.8 and 0.4 to 3.2 mg m^{-2} respectively) compared to fucoxanthin (20.9 to 160.2 mg m^{-2}) clearly evidence the dominance of diatoms over the other classes of phytoplankton all over the study area, except at R and TNS1. At these stations, Chl *a* : 19′BF (12.0 ± 1.4), and Chl *a* : 19′HF (4.4 ± 0.1) ratios were the lowest of the study area, reflecting the higher contribution of nanoflagellates to the phytoplankton community (data not shown).

3.1.2 Vertical distributions along transects TNS and TEW

The vertical distribution of Chl *a* along transects TNS and TEW are presented in Figs. 3 and Fig. 4 respectively. For both transects, the higher concentrations (> 0.5 mg m^{-3})

BGD
11, 8259–8324, 2014

were restricted to the upper 150 m and were clearly dominated by microphytoplankton communities.

At the beginning of the bloom, Chl *a* concentrations ranged from 0.5 to 1.5 mg m^{-3} in the upper 150 m along the TNS transect (Fig. 3). TNS1 was very different from the rest of the transect with higher contributions of nanophytoplankton over 150 m (20 to 50 % contribution to total biomass depending on depth; Fig. 5). Ten days later, higher phytoplankton biomasses (up to 5.0 mg m^{-3}) were observed in the PF area between TEW7 and TEW8 (Fig. 4). Vertical profiles clearly evidenced the PF influence which isolated very high Chl *a* waters to the north from comparatively lower Chl *a* waters to the south. The coastal station TEW1 was also characterized by very high Chl *a* concentrations within the first 40 m (up to 4.7 mg m^{-3}). As shown by satellite images (d'Ovidio et al., 2012), TEW1 already supported a large phytoplankton bloom before the beginning of the cruise, likely due to precocious favorable growth conditions in the coastal zone. The latter was separated from the off–plateau waters by the southern branch of the PF circulating along the shelf-break between TEW3 and TEW4. The PF signature along the shelf break was defined by lower Chl *a* concentrations (< 1.0 mg m^{-3}). Maximum concentrations in fucoxanthin (2.0 to 2.5 mg m^{-3}) were similarly found for both the eastern area north of the PF and at station TEW1, indicating the dominance by diatoms (Fig. 6). The core of the TEW transect (TEW4 to TEW6) was characterized by Chl *a* concentrations ranging from 1.0 to 1.5 mg m^{-3} at the surface and a significant increase of the nanophytoplankton contribution to the total biomass (20 to 30 %; Fig. 6). An increased grazing activity was evidenced at TEW7 and TEW8 by relatively higher concentrations in phaeopigments (Phaeo); the ratio of Phaeo to Chl *a* was indeed higher (0.3) at these sites as compared to all other stations (< 0.1; data not shown).

3.1.3 Temporal evolution at contrasted productive stations

No clear temporal evolution of the phytoplankton biomass could be evidenced in the complex system of recirculation located in the stationary meander of the PF,

BGD
11, 8259–8324, 2014

as demonstrated by the integrated Chl *a* concentrations (ranging between 98.2 and 129.0 mg m^{-2}) at stations E1 to E5 in Fig. 7.

Stations E4W and A3 were visited two times (Fig. 7). The largest phytoplankton development was observed at the KP reference station A3, where Chl *a* concentrations have increased 3.5-fold over one month (from 106.2 mg m^{-2} in October, A3-1 visit, to 371.7 mg m^{-2} in November, A3-2 visit). This evolution was accompanied by an increase of the Phaeo : Chl *a* ratio (from < 0.1 to 0.3), reflecting a higher grazing activity at the second visit (data not shown).

Station E4W was characterized by a moderate evolution compared to A3, likely due to the shorter period of time between the two sampling periods (6 days compared to 27 days). Chl *a* concentrations increased about 2-fold from 131.2 to 249.8 mg m^{-2} between the two visits.

For A3 station and E stations, the temporal evolution of chlorophyll biomass was mainly due to the development of a microphytoplankton community largely dominated by diatoms. At these stations, integrated nano- and picophytoplankton biomasses, determined using diagnostic pigments, were very low and nearly constant all over the course of the cruise (respectively 14.4 ± 3.7 and 4.6 ± 1.7 mg m^{-2}; Fig. 7).

3.2 Biogenic silica and particulate organic matter

3.2.1 Spatial variability over the study area

The study area was characterized by an heterogeneous distribution of biogenic silica (BSi) and particulate organic carbon (POC), nitrogen (PON) and phosphorus (POP) (Fig. 8). The lowest vertically integrated concentrations of BSi, POC, and PON were measured at the off-shore stations R and TNS1 with integrated values over 200 m of 88.6 mmol Si m^{-2}, 610.5 mmol C m^{-2}, and 78.1 mmol N m^{-2} respectively. The lowest concentrations of POP were evidenced at the station TEW3 (8.9 mmol P m^{-2} over 200 m). The highest concentrations were observed between TEW7 and TEW8 (250.4 to 377.6 mmol Si m^{-2} for BSi, 1200 to 1875 mmol C m^{-2} for POC, 214.7 to

BGD
11, 8259–8324, 2014

354.4 mmol N m^{-2} for PON, 29.5 to 39.0 mmol P m^{-2} for POP), confirming the very high phytoplankton biomass of the PF area. North of the KP, the distribution of BSi, POC, PON and POP was influenced by the passage of the PF which isolated northern waters characterized by low particulate matter concentrations from southern waters characterized by high particulate matter concentrations. This feature is especially highlighted for BSi concentrations (Table 1).

3.2.2 Vertical distribution along transects TNS and TEW

At the beginning of the bloom, along the TNS transect, POC, PON and POP concentrations were low at all stations (< 12 µmol C L^{-1}, < 1.5 µmol N L^{-1} and < 0.16 µmol P L^{-1} respectively; Fig. 9). For BSi concentrations, two contrasted areas were observed on either side of the PF, with southern waters richer (1.29 to 3.14 µmol Si L^{-1}) than northern waters (0.08 to 1.05 µmol Si L^{-1}).

Along the TEW transect (Fig. 10), ten days later, the vertical distributions of BSi and particulate organic matter clearly followed the same pattern as Chl *a*. The highest BSi, POC, PON and POP concentrations were observed at both the coastal station TEW1 at the surface (2.77 to 5.87 µmol Si L^{-1}, 5.50 to 16.3 µmol C L^{-1}, 1.00 to 2.82 µmol N L^{-1}, and 0.15 to 0.22 µmol P L^{-1} respectively) and in the PF area between TEW7 and TEW8 down to 50 m depth (2.85 to 5.42 µmol Si L^{-1}, 10.1 to 31.9 µmol C L^{-1}, 2.42 to 5.89 µmol N L^{-1}, 0.23 to 0.81 µmol P L^{-1} respectively). The core of the transect (TEW3 to TEW6) was characterized by lower particulate matter concentrations (0.51 to 2.91 µmol Si L^{-1}, 3.93 to 11.4 µmol C L^{-1}, 0.42 to 2.21 µmol N L^{-1} and 0.01 to 0.19 µmol P L^{-1}). As noticed for Chl *a* in this area, higher BSi concentrations (2.32 to 2.91 µmol Si L^{-1}) were observed at TEW4 down to 100 m depth. Standing out of Chl *a* and particulate organic matter distributions, a well-defined deep BSi maximum (2.00 ± 0.10 µmol Si L^{-1}) was found at 300 m at TEW5.

For both transects, the vertical distribution of BSi strongly paralleled that of fucoxanthin (Fig. 3), confirming the dominance of diatoms in the phytoplankton communities of

BGD
11, 8259–8324, 2014

the Kerguelen region. Size-fractionation of BSi can bring information on the sizes of the diatoms even though the presence of debris can alter this information. Nano-sized fraction of BSi (0.8 to 20 µm) can then correspond to the presence of small diatom species or fragments of diatoms. Micro-sized fraction of BSi (> 20 µm) indicates the presence of large siliceous phytoplankton which could represent both large diatoms cells and large colonies of diatoms. In the Kerguelen region, size fractionation of BSi (Fig. 11) revealed the major role played by large (> 20 µm) siliceous phytoplankton which accounted for > 60 % of total BSi at all productive stations over different depths according to the location: down to 200 m at TEW4, A3-2, and E (E1 to E5) stations (typical vertical profile represented by station TEW4 in Fig. 11a), down to 100 m at E4W and in the PF area (represented by FL vertical profile in Fig. 11b), and down to 40 m at TEW1 (data not shown). The relative contribution of the two size classes was mainly driven by the evolution of the large size fraction over these different depths, as the small size fraction concentrations remained fairly constant around 190 mmol Si m^{-2}. As a consequence, the nano-sized diatoms (0.8 to 20 µm) were dominant at the low productive stations (R, TNS1, TNS2, TEW2, TEW3, TEW5 and TEW6; typical vertical profile illustrated by station R in Fig. 11c) and everywhere below 200 m except at station TEW5 (Fig. 11d). The latter station showed an increasing contribution of the micro-sized fraction (> 20 µm) to total siliceous biomass with depth (ranging from 23 % at the surface and 60 % between 300 and 400 m). This unusual feature coincided with the deep BSi maximum mentioned above.

3.2.3 Temporal evolution at contrasted productive stations

Slight increases in BSi (Fig. 12) and particulate organic matter (data not shown) concentrations were observed at stations E. From E1 to E3, integrated concentrations over 200 m were relatively constant (average: 308.2 ± 23.6 mmol Si m^{-2} for BSi, 1065 ± 51 mmol C m^{-2} for POC, 195.6 ± 11.6 mmol N m^{-2} for PON and 13.5 ± 1.6 mmol P m^{-2} for POP). Values then increased at E4E and E5, reaching 410.7 ± 23.1 mmol Si m^{-2}, 1651 ± 26 mmol C m^{-2}, 231.5 ± 31.0 mmol N m^{-2} and 28.5 ±

BGD
11, 8259–8324, 2014

5.9 mmol P m^{-2}. In addition, vertical profiles revealed that BSi and particulate organic matter were concentrated in a shallow layer (from the surface down to 100 m depth) during these two last visits (data not shown).

As mentioned for Chl *a*, the largest phytoplankton development was observed at A3 with increasing concentrations of BSi (from 163.5 to 713.3 mmol Si m^{-2}), POC (from 1259 to 2267 mmol C m^{-2}), PON (from 137.9 to 435.9 mmol N m^{-2}), and POP (from 9.7 to 29.3 mmol P m^{-2}) between A3-1 and A3-2 visits (Fig. 12, data not shown for POC, PON and POP concentrations). On the first visit of E4W, the situation was already characterized by high BSi, POC, PON, and POP concentrations over 100 m depth (up to 3.83, 20.0, 3.60, 0.27 µmol L^{-1} respectively). The temporal evolution between the two visits was still considerable with integrated concentrations varying from 379.5 to 744.2 mmol m^{-2} for BSi, 1162 to 1598 mmol m^{-2} for POC, from 288.2 to 354.1 mmol m^{-2} for PON, and from 21.5 to 32.6 mmol m^{-2} for POP.

The temporal evolution of particulate matter in the meander of the PF and at stations A3 and E4W evidenced a significant growth of the siliceous phytoplankton community since the beginning of the cruise. As a general trend, the large size fraction (> 20 µm) was overall contributing to around 60 % of integrated BSi stocks in the surface productive layer, with the exception of stations R and E3 where the small size fraction (0.8 to 20 µm) was slightly dominant (respectively accounting for 59.4 % and 52.5 % of above mentioned integrated BSi stocks). However, it is particularly important to notice that the BSi stocks located between 200 and 400 m, which may reflect the communities sinking out of the surface layer, were always dominated by the nano-sized particles (ranging from 61.4 to 86.1 % of BSi stocks integrated from 200 to 400 m depths).

3.3 Elemental ratios of particulate matter

The elemental ratios in the upper 200 m are presented as six clusters of stations (Fig. 13), grouped in function of biomass, elemental ratios and phytoplankton community structure reported for each station. The objective of this clustering is to provide

BGD
11, 8259–8324, 2014

an overview of the distribution of elemental ratios over the study area to highlight some spatial and temporal patterns. Each cluster of stations includes systems with different environmental dynamics. Mann–Whitney tests were then performed on these six clusters for each elemental ratio (Si : C, Si : N, Si : P, C : N, C : P and N : P) to determine the clusters that were significantly different from each other at the 95 % confidence level (Fig. 13). The six clusters of stations corresponded to: (1) the lowest biomass stations including the off-plateau stations R and TNS1, and A3-1 at the start of the bloom, (2) the moderate productive stations north of the PF (TNS2, TEW2, TEW3), (3) the high biomass stations in the PFZ (TEW7, TEW8, FL, FS), (4) the high biomass stations south of the PF (A3-2, E4W, E4W2), (5) the moderate biomass stations south of the PF (TNS3 to TNS10, E1 to E5, TEW4 to TEW6), (6) the coastal station TEW1.

The lowest Si : C, Si : N and Si : P ratios were observed at the lowest biomass stations (cluster (1)) of the study area in the upper 200 m (respectively 0.11 ± 0.07, 0.67 ± 0.43 and 9.6 ± 6.4). Except for cluster (1), Si : C, Si : N and Si : P ratios were always higher than the typical values for nutrient–replete diatoms (Brzezinski, 1985). The highest average values were observed at the coastal station TEW1 in the upper 70 m (cluster (6)) reaching 0.70 ± 0.25 for Si : C, 2.59 ± 0.40 for Si : N and 34.4 ± 6.6 for Si : P. The other stations located north of the PF or in the PFZ (clusters (2) and (3)) were characterized by lower average Si : C, Si : N and Si : P molar ratios (respectively 0.28 ± 0.01, 1.32 ± 0.13, 16.0 ± 2.6) than the stations south of the PF (respectively 0.35 ± 0.01, 1.75 ± 0.05, 24.9 ± 4.3). This observation agreed with statistical tests: the clusters of the stations north of the PF were statistically different from the other clusters south of the PF (Fig. 13).

Except for the lowest biomass stations (cluster (1)), C : N and C : P ratios were relatively constant (reaching average values of 5.1 ± 1.4 and 73.0 ± 35.4 respectively) and lower than the Redfield et al. (1963) ratios. N : P ratios were close to the Redfield's ratio all over the study area (average: 14.4 ± 6.3) except for the stations located in the PFZ (cluster (3)). These stations were characterized by lower C : P ($48.1.7 \pm 18.0$) and N : P (10.5 ± 3.3) ratios than the rest of the study area. The Mann–Whitney test did not

BGD
11, 8259–8324, 2014

evidence any significant difference between the median of the six clusters for C : P and N : P ratios. For C : N ratios, only the low biomass stations were significantly different from the other stations at the 95 % confidence level.

Over the course of the cruise, the development of diatoms was evidenced between the first (A3-1) and the second visits (A3-2) at A3 with Si : C and Si : N ratios increasing respectively from 0.14 ± 0.06 to 0.32 ± 0.06 and 0.87 ± 0.25 to 1.66 ± 0.24 (data not shown). Significant increases in Si : C and Si : N were also observed at E4W from the first (0.29 ± 0.12 for Si : C and 1.25 ± 0.62 for Si : N) to the second visit (0.39 ± 0.07 for Si : C and 2.06 ± 0.15 for Si : N). Moderate increases were shown for Si : P ratio both at A3 (from 17.3 ± 2.9 to 19.6 ± 6.7) and E4W (from 18.3 ± 4.4 to 19.4 ± 6.3). At E4W, a slight decrease was evidenced from the first to the second visit for C : N (from 5.5 ± 0.5 to 5.0 ± 0.5), C : P (from 76.3 ± 12.3 to 71.7 ± 25.7) and N : P (from 17.1 ± 6.0 to 12.9 ± 1.9). At A3, higher decrease was observed from the first to the second visit for C : N (from 8.8 ± 3.5 to 5.3 ± 0.2), C : P (from 148.9 ± 47.2 to 65.9 ± 32.8) and N : P (from 20.9 ± 3.1 to 11.4 ± 5.2).

3.4 Lithogenic silica

Lithogenic silica is a good proxy to track the transport of lithogenic material (and indirectly Fe) from terrestrial erosion, aeolian dust deposition or sediment resuspension to the water column (Quéguiner et al., 1997). Over the entire study area, LSi concentrations did not exceed 0.11 $\mu mol\,L^{-1}$ throughout most of the water column, except at stations subjected to continental influence (Fig. 14). The highest LSi values were observed at the coastal station TEW1 (average: $1.31 \pm 0.14\,\mu mol\,L^{-1}$) and at station A3 near the bottom ($1.34 \pm 0.07\,\mu mol\,L^{-1}$). In addition, compared to surrounding waters, station A3 was characterized by relatively higher concentrations down to 300 m (values $> 0.15\,\mu mol\,L^{-1}$). This feature was also observed at the second visit A3-2 (Fig. 15). The lowest LSi concentrations were found at TNS1 with values $< 0.01\,\mu mol\,L^{-1}$ over the first 400 m (Fig. 14). As expected, concentrations were low at station R (Fig. 15), located far from any continental influence ($< 0.04\,\mu mol\,L^{-1}$ in the upper 100 m), al-

BGD
11, 8259–8324, 2014

though a maximum was reported at 500 m (0.12 µmol L^{-1}). The stations E located in the complex system of recirculation showed LSi concentrations < 0.10 µmol L^{-1} but local maximums (0.12 to 0.13 µmol L^{-1}) between 600 and 700 m were noticed at E1, E4E and E5 (and likely E2, although data are missing to confirm it). High LSi concentrations were also observed at E4W at 75 m and 400 m (0.23 and 0.12 µmol L^{-1} respectively) only during the second visit. Along the transect TEW, LSi concentrations were higher in the PFZ reaching values higher than 0.11 µmol L^{-1} over the water column at TEW8.

As a general trend, LSi was mainly composed of small particles (from 0.8 to 20 µm) over the water column, representing in average 59.5 % of total LSi. However, local maximums observed at A3-2 (50 m), FL (300 m), E4W2 (75 and 400 m) and E5 (600 m) were associated to large particles (> 20 µm), accounting for 65.2 to 86.5 % of the total LSi.

4 Discussion

4.1 The Kerguelen Plateau region: a mosaic of biogeochemical environments

The biogeochemical characteristics of the water masses northeast of the Kerguelen Islands have already been documented by Blain et al. (2001) in early spring (October 1995). They highlighted the complex mesoscale structure of water masses which generated contrasting biogeochemical environments above the KP. The particular mesoscale circulation is directly impacted by the topography of the KP and the presence of the PF pathway isolating warm northern subantarctic surface waters from cold southern Antarctic Surface Water (AASW) (Park and Gamberoni, 1997). Similar circulation patterns (Park et al., 2014; Zhou et al., 2014) were observed during the KEOPS2 cruise. This is probably partly for that reason that a mosaic of biogeochemical conditions was also encountered.

BGD
11, 8259–8324, 2014

Coastal waters (corresponding to stations TEW1 and TEW2) were characterized by a large diatom bloom and high LSi concentrations, evidencing strong lithogenic material inputs (including iron) from the plateau.

A strong shelf front isolated these warmer coastal waters (> 2.4 °C) from the cold (2.3 °C) PF water tongue containing low Chl *a* and BSi concentrations. Blain et al. (2001) associated this water tongue (corresponding to station TEW3 in our study) to an intrusion of AASW where phytoplankton growth was limited by an unfavorable light-mixing regime. Indeed, TEW3 showed the deepest mixed layer depth (95 m) of the west-east transect, but unfortunately photosynthetic parameters were not determined precluding any conclusion about the light limitation hypothesis. Grazing pressure could also be another limiting factor for phytoplankton growth. However, zooplankton biomass was too low at TEW3 (Carlotti et al., 2014) to explain the low Chl *a* and BSi concentrations.

By contrast, a productive, high–biomass system was found in the eastern area in the PF between TEW7 and TEW8. This area was characterized by a shallow mixed layer (down to 50 m), likely providing favorable light conditions for diatom growth. Despite being far from the plateau, these stations showed sufficient iron concentrations ($\sim 0.2\,\mathrm{nmol\,L^{-1}}$ over 50 m; Quéroué et al., 2014) to support phytoplankton growth. Significant iron could be supplied by the transport of Fe-rich deep waters from the KP to the northwestern Kerguelen Abyssal Plain east of the KP (Zhou et al., 2014), but also from the coastal area by lateral advection driven by the subantarctic surface water eastward flow north of the PF (Bucciarelli et al., 2001). Potential sources of iron will be discussed in Sect. 4.4.

The largest diatom development was observed over the southeast KP at the reference station A3 (during the second visit) with the highest Chl *a* and BSi concentrations reported during the cruise. This station also evidenced high LSi concentrations near the bottom suggesting lithogenic material inputs from the plateau sediments. Indeed, one major conclusion of KEOPS1 was that the long-lasting diatom bloom above the plateau was maintained by the continuous supply to the surface mixed layer of iron

BGD
11, 8259–8324, 2014

and nutrients. The latter originated from below due to an enhanced tidally–induced vertical mixing associated to a weak mean residual circulation resulting in a long retention time for nutrients and trace elements (Blain et al., 2007; Park et al., 2008a). On a longer time–scale, it was assumed that iron supply to A3 originated from horizontal advection from the extensive shoal around the Heard/Mc Donald Islands (Park et al., 2008a). East of the KP, this northward circulation along the topography could also lead to a partial export of the plateau bloom. This feature was supported by the observation of similar biogeochemical properties at station A3 and at the eastern flank (corresponding to station E4W for the two visits) of the KP. The E4W station evidenced the same range of values as A3 in terms of BSi, POC, PON, and POP concentrations and quite similar diatom community compositions mainly dominated by *Chaetoceros* subgenus *Hyalochaete*, *Pseudo-nitzschia* spp., and *Thalassiosira* spp. (Lasbleiz et al., 2014). Furthermore, the assemblages in sediments at these two sites were similarly composed of *Eucampia antarctica*, *Dactyliosolen antarctica*, *Fragilariopsis kerguelensis*, *Chaetoceros* resting spores, *Rhizosolenia* spp. as well as an uncommon species, *Thalassiosira decipiens*, not observed anywhere else over the study area (Wilks, 2013). The northward export of part of the southeast KP bloom also serves as a good explanation to the higher particulate matter concentrations observed at TEW4 compared to the other stations of the TEW transect at the beginning of the cruise.

As compared to the easternmost part of the study area in the PF, the stations south of the PF exhibited moderate biomasses. Inside the meander of the PF, two stages in the development of the siliceous phytoplankton community were observed in the course of the cruise. At the beginning, particulate matter concentrations were moderate and slightly decreasing from E1 to E3. The microplanktonic size fraction (> 20 µm) contribution to siliceous biomass was also decreasing while the nanoplanktonic size fraction contribution increased from 34.5 % at E1 to 47.5 % of the siliceous biomass at E3. By contrast, the two last visits (E4E and E5) showed an increase in phytoplankton biomass dominated by large diatoms and concentrated over a shallower depth. Closset et al. (2014) also reported these two contrasted periods through the $\int D : P$ ratio

BGD
11, 8259–8324, 2014

defined as the ratio of Si dissolution rates (D) to Si production rates (P) integrated over the euphotic zone. From E1 to E3, increasing $\int D : P$ ratio evidenced an increased BSi loss due to enhanced BSi dissolution in surface waters, while decreasing $\int D : P$ ratio between E4E and E5 resulted from enhanced BSi production rates and revealed bloom conditions. Together, these results would suggest that the start of the bloom period (E4E and E5) was preceeded by a non-lasting phytoplankton development before the first sampling (E1). This short bloom event could have been aborted by adverse hydrodynamic conditions before the beginning of the cruise. This was consistent with the increase in the proportion of empty diatoms frustules from E1 to E3 (from 5.1 % to 25.7 %; Lasbleiz et al., 2014) and the increase of phytodetrital and fecal aggregates observed at depth by Laurenceau et al. (2014). The important role of mesoscale structures and turbulence in the control of primary production and light availability have already been reported by previous studies (e.g. Lancelot et al., 2000; Lévy et al., 2001; Read et al., 2007). We hypothesize that the instability of the mixed layer depth before the beginning of the cruise could have generated deepening events providing unfavourable light conditions for phytoplankton growth. Our hypothesis is supported by the σ_Θ profiles which indicate the existence of a secondary pycnocline around 130 m at E1 and a continuous gradient with no clear mixed layer from the surface down to 200 m depth at E3 (data not shown). Furthermore, the slight increase in zooplankton abundance from E1 to E3 (Carlotti et al., 2014) suggests that phytoplankton growth was not mainly impacted by grazing pressure. Another feature of the area south of the PF was the presence of a minimum of biomass in the central core of the complex recirculation meander (corresponding to station TEW5). This central core stands out from the rest of the study area by the presence of a deep silica maximum (between 300 and 400 m) mainly associated to microplanktonic size particles (> 20 µm). There could be several explanations for this peculiar feature. (1) Given the low Si biomass at the surface, the presence of large and non-living diatoms at depth could reflect the sedimentation of an early bloom that could have been quickly driven to an end due to adverse hydrodynamic conditions, as discussed above. A vertical net haul down to 100 m depth at

BGD
11, 8259–8324, 2014

TEW5 revealed the dominance of the heavily silicified diatoms *Fragilariopsis kerguelensis* as well as *Corethron pennatum* (L. Armand, personal communication, 2013). However no sediment sample was collected at this station to evidence their eventual influence on vertical export. (2) Mesoscale activity could also have favored the transfer and the accumulation of biogenic silica at depth in the central meander area which is characterized as a region of general downwelling (Zhou et al., 2014). (3) Finally, the northward circulation from the KP could have advected large and non-living diatoms already sedimenting at depth coming from productive southern waters.

Overall, our results highlighted the presence of a mosaic of biogeochemical situations revealed by the five contrasted areas over the KP in the early spring. At this time of the year, both light-mixing regime and grazing would control phytoplankton growth in these iron and nutrient replete waters (Blain et al., 2014; Carlotti et al., 2014; Quéroué et al., 2014). The first three situations are similar to what was observed by Blain et al. (2001): (1) a productive coastal area subject to strong lithogenic (and thus iron) inputs (from TEW1 to TEW2), (2) a water tongue likely limited by light availability (TEW3) and (3) a productive site in the easternmost study area in the PF (from TEW7 to TEW8). The two other situations are represented by (4) the highest productive site A3 over the southeastern KP already observed during KEOPS1 (Blain et al., 2007) and (5) a delayed phytoplankton development strongly influenced by the mesoscale activity of the complex system of recirculation in the meander of the PF (E stations).

4.2 Impact of natural iron enrichment on Chl a and phytoplankton communities

4.2.1 The off-plateau HNLC stations

During the KEOPS2 cruise, the off-plateau station R showed the lowest chlorophyll biomass (39.0 mg m^{-2}) despite high macronutrient concentrations of the surrounding waters (Blain et al., 2014). In this HNLC area, one limiting factor was likely iron availability as suggested by the low iron concentrations in surface waters (~ 0.1 nmol L^{-1}; Quéroué et al., 2014) and the Fe–Cu incubation experiments (Bowie et al., 2014;

BGD
11, 8259–8324, 2014

Sarthou et al., 2014). Light could also have been (co-)limiting as the mixed layer extended down to ∼120 m almost exactly coinciding with the 0.01 % surface light level. Chl *a* concentrations were in the same order of magnitude as that measured in typical HNLC waters of the Southern Ocean (Bathmann et al., 1997; Gall et al., 2001; Froneman et al., 2004) and more specifically, of the Kerguelen region (Cailliau et al., 1997; Uitz et al., 2009). Integrated chlorophyll biomass was however higher than the lowest values corresponding to the poorest areas of the Southern Ocean (range: 10 to 20 mg m^{-2}) suggesting the slight phytoplankton development that may have occurred shortly before the site visit. In contrast to the other stations of the study area, the off-plateau station R showed a lower microphytoplankton contribution (47 % of total Chl *a* biomass) due to a higher proportion of nanophytoplankton (39 % of total Chl *a* biomass). This result was expected from previous artificial and natural iron-fertilization experiments (Gall et al., 2001; Hoffmann et al., 2006; Moore et al., 2007; Lance et al., 2007). Increased contributions of nano-sized communities (small diatoms or flagellates) were reported under iron limited conditions (Sunda and Huntsman, 1997; Timmermans et al., 2001; Armand et al., 2008; Uitz et al., 2009). Cell counts confirmed the dominance of nanoflagellates at station R in terms of C biomass (Lasbleiz et al., 2014). Several species of dinoflagellates and the silicoflagellate *Dyctiocha speculum* were also important contributors to C biomass compared to diatoms. At station R, the Chl *a* : Fuco ratio (3.7) and Chl *a* : 19′BF ratio (11.0) were respectively higher and lower than those measured for diatoms (Wright and Jeffrey, 1987; Ediger et al., 2001). Such Chl *a* : Fuco and Chl *a* : 19′BF ratios have been reported for dinoflagellates in previous studies (Johnsen and Sakshaug, 1993; Ediger et al., 2001).

Like the station R, the off-plateau station TNS1 was distinguished from the study area by its low chlorophyll biomass (52.1 mg m^{-2}) and higher proportion of nano- (41 %) and pico- (20 %) phytoplankton. Even if there are no available data to confirm it, a limitation by iron seems almost likely given the tenuity of the surface mixed layer (from 20 to 35 m), the high abundance of macronutrients (Blain et al., 2014) and the low grazing pressure (Carlotti et al., 2014). At station R and TNS1, the picophytoplankton contribu-

BGD
11, 8259–8324, 2014

tion to chlorophyll biomass was higher (up to 20 %) than in the rest of the study area but relatively low by comparison to previous studies in HNLC waters (Kopczyñska et al., 1998; Gall et al., 2001). Similar results were reported for the HNLC station of the first cruise KEOPS1 (Uitz et al., 2009).

4.2.2 The iron-fertilized stations

By contrast, larger developments of phytoplankton were observed in the iron-fertilized Kerguelen region, confirming the classical stimulation of phytoplankton growth under iron-replete conditions (Martin, 1990). Integrated chlorophyll biomass ($152.5 \pm 77.4\,mg\,m^{-2}$) fell in the range typically reported for different regions of the Southern Ocean (Peeken, 1997; Wright and van den Enden, 2000; Uitz et al., 2009). Some very high productive stations (A3-2, E4W2 and the area from TEW7 to TEW8) were comparable to the highly productive regions like the Ross sea (Goffart et al., 2000), reflecting the high productivity of the early bloom. The large development of diatoms was notably evidenced at station A3 where Chl *a* biomass increased 3.5-fold from October to November.

All over the iron-fertilized area, chlorophyll biomass was largely dominated by large diatoms (> 20 µm), as suggested by the higher concentrations in fucoxanthin over the other pigments. Previous artificial iron-fertilization experiments reported the shift from nano- and/or picophytoplanktonic communities to large diatoms (> 20 µm) after Fe-addition (Gall et al., 2001; Hoffmann et al., 2006; Lance et al., 2007). The dominance of large diatoms was also observed in other natural Fe-fertilized regions of the Southern Ocean (Bathmann et al., 1997; Moore et al., 2007; Uitz et al., 2009).

Interestingly, relatively high Chl *a* biomasses were found below the mixed layer all over the iron-fertilized area. This feature was also observed during KEOPS1 at the Plateau reference station A3 and resulted in the progressive formation of a deep chlorophyll maximum (DCM) associated to a deep biogenic silica maximum at 125 m (Mosseri et al., 2008; Uitz et al., 2009). Uitz et al. (2009) explained this DCM by the accumulation of inactive but living algal cells at the deep temperature-driven pycnocline. During

BGD
11, 8259–8324, 2014

KEOPS2, a second density gradient (identified from the σ_Θ profiles) deeper than the MLD was observed for most of the stations over the iron-fertilized area. Furthermore, Si-production by diatoms was lower but still observed below the mixed layer although irradiance levels were < 1 % PAR (Photosynthetically Active Radiation; Closset et al., this issue; Lasbleiz et al., 2014). The acclimation of phytoplankton to low light levels has already been reported by Cullen (1982) and more recently by Banse (2004) and Marra et al. (2014). In addition, cell counts revealed that the community composition was rather the same within and beneath the mixed layer, with the difference that the proportion of empty cells was higher beneath the mixed layer. These observations would suggest that Chl *a* biomass below the mixed layer would result from the sedimentation of living diatoms from the upper layer rather than in situ growth of a specific deep-dwelling community. Characterized by low light levels and high nutrient concentrations, the layer between the surface mixed layer and the second pycnocline would also allow a slight growth of phytoplankton. Thereafter, this accumulation of sinking cells could be enhanced by the shift of phytoplankton communities towards more heavily silicified diatoms, observed later in the season by Armand et al. (2008). Together all these observations could explain the occurrence of the DCM observed at the Plateau reference station A3 during the demise of the bloom (Uitz et al., 2009).

4.3 Element composition and stoichiometry

4.3.1 Si, C, N, P stocks

Above 200 m, the iron-fertilized stations were characterized by the progressive development of micro-sized diatoms (> 20 µm) resulting in high biogenic silica and particulate organic matter concentrations at some productive stations (A3-2, E4W2, and the area from TEW7 to TEW8). These high concentrations fell in the range of those measured in the PFZ in spring (Quéguiner et al., 1997; Brzezinski et al., 2001; Quéguiner and Brzezinski, 2002). At the HNLC reference station, BSi stocks were clearly lower due to a higher proportion of nanoflagellates (39 %).

BGD
11, 8259–8324, 2014

Below 200 m, the biogenic silica (especially at A3, E4W, TEW7 and TEW8) was dominated by the smaller (0.8 to 20 µm) size fraction despite the development of large diatoms in surface waters. This could either reflect the sedimentation of small diatoms coming from a short bloom event before sampling or/and an active degradation of diatoms at the top of the mesopelagic zone inducing the fragmentation of siliceous planktonic particles by grazers. Given that organic matter is preferentially degraded relative to biogenic silica, the hypothesis of an enhanced degradation from 200 m and beyond could explain the low POC export reported by Planchon et al. (2014) who also report elevated $^{234}Th:^{238}U$ ratios slightly > 1 in between 250 and 700 m at E3 and in between 200 to 600 m at E5. Similarly, Jacquet et al. (2014) report a Ba_{xs} maximum centered around 400 m at E3 and E5 which indicates an increased remineralisation of organic matter. From various sediment trap deployments at 200 m depth, Laurenceau et al. (2014) evidenced a negative correlation between primary productivity and export efficiency, suggesting that the highest productive stations were the least efficient to carbon export.

4.3.2 Elemental stoichiometry Si : C, Si : N and Si : P in particulate matter

Both artificial and natural iron-fertilization experiments have documented the influence of iron on the elemental ratios of phytoplankton communities (Hutchins and Bruland, 1998; Takeda, 1998; Franck et al., 2000; Hare et al., 2007; Moore et al., 2007). They usually mention higher (2 to 3 times) Si : C, Si : N and Si : P ratios under Fe-stress as compared to values under Fe-replete conditions (Si : C = 0.13, Si : N = 1.1; Brzezinski, 1985). This is supposed to indicate the development of more heavily silicified diatoms under iron-stress (Hutchins and Bruland, 1998; Takeda, 1998). Surprisingly, we report here an opposite trend: the iron-fertilized stations mentioned above evidenced 2-fold higher Si : C and Si : N ratios than those of the HNLC station R (close to Brzezinski's ratios). The high Si : C and Si : N ratios observed at the iron-fertilized stations could be explained by a differential recycling of organic matter and biogenic silica, and/or increased Si requirements by the dominant species. Bacterial activity and grazing pres-

BGD
11, 8259–8324, 2014

sure by zooplankton could explain the preferential degradation of soft organic matter over BSi dissolution in surface waters. However, in the early productive period, their impact on particulate matter stoichiometry is probably not yet significant: Christaki et al. (2014) indicates that a few pourcent of primary production (gross community production; Cavagna et al., 2014) at A3 are channeled through the microbial loop and the mesozooplankton.

The high Si : C, Si : N and Si : P ratios of the productive stations would then rather indicate the presence of phytoplankton communities dominated by heavily silicified diatoms. Our interpretation agrees with the high Si uptake rates, compared to C and N uptake rates, measured at A3, E4W and FL (located between TEW7 and TEW8) by Closset et al. (2014). These results are consistent with Si : C production ratios reported for the PFZ during austral spring and reaching values as high as 0.45 in the Pacific sector (Brzezinski et al., 2001) and 0.32 to 1.19 in the Atlantic sector (Quéguiner and Brzezinski, 2002). However, while these authors attribute the strong silicification to limitation by iron, it seems, in our instance, that the ratios we observe during the early blooms are rather related to the taxonomic composition of diatom assemblages. It is interesting to notice that the highest Si : C ratio of 1.19, reported by Quéguiner and Brzezinski (2002), was observed during the early stage of a bloom development dominated by *Corethron criophilum* and *Fragilariopsis kerguelensis,* and that the Si : C ratio then decreased to the lower value of 0.32 later in the season. Our observations would thus suggest that biogenic particulate matter at the onset of the blooms of naturally iron–fertilized environments could be typically Si enriched compared to C, N and P, due to the presence of specific diatom communities. Our finding is a major difference between the experiments of natural fertilization and artificial fertilization in the Southern Ocean. In the latter, diatoms that grow are often referred to as opportunistic species such as *Pseudo-Nitzschia* spp. and *Chaetoceros* spp. and these taxa are also those involved in the pioneer works of Hutchins and Bruland (1998) and Takeda (1998). Apart from this general trend, the European Iron Fertilisation Experiment (EIFEX) did not evidence the classical decrease of Si : C and Si : N ratios observed in artificial iron-

BGD
11, 8259–8324, 2014

experiments (Hoffmann et al., 2006; Smetacek et al., 2012). Initial Si : C, Si : N and Si : P elemental ratios (respectively 0.24, 1.5 and 18.0) increased from 1.8 to 2.6 times in 37 days after the first fertilization. This feature was attributed to a shift, more pronounced compared to the other artificial fertilization studies, towards more heavily silicified diatom species. Furthermore, the laboratory cultures of two Southern Ocean diatom species (*Fragilariopsis kerguelensis* and *Chaetoceros dichaeta*) highlighted the species-specific response to iron availability in the elemental composition (Hoffmann et al., 2007). Under natural conditions, the control of stoichiometric ratios is thus more complex and depends largely on the diatom community structure, itself depending on the dominant species adapted to their specific set of environmental conditions.

Although surprising at first sight, the low Si : C and Si : N ratios observed at R are explained by the dominance of non-siliceous organisms (mostly nanoflagellates) decreasing Si proportion compared to C and N in the bulk particulate matter. Diatoms contribution to C biomass was however significant (representing 34 % of the particulate organic carbon at the surface; Lasbleiz et al., 2014) which could reflect a short development of a diatom assemblage just prior our sampling. This is consistent with the high dissolution rates of BSi observed in surface waters (Closset et al., 2014) and the high mineralization activity evidenced in the mesopelagic zone (Jacquet et al., 2014). It is likely that particular biogeochemical conditions characterizing the start of the productive period would have induced a progressive shift in the community composition. At the end of winter, the reference station R would be characterized by high-nutrient waters, and unfavorable light conditions for diatom growth. By early spring, iron concentrations were relatively low but likely sufficient to trigger a short phytoplankton growth as soon as light conditions became favorable. Given the low iron winter stock available, the bloom quickly stops well before the diatoms have had time to use the stock of macronutrients. This would induce optimal conditions to the development of heterotrophic communities, able to grow on the decaying bloom of diatoms.

BGD
11, 8259–8324, 2014

4.3.3 Elemental stoichiometry C : N, C : P and N : P in organic particulate matter

During KEOPS2, we observed a consistently lower N : P ratio compared to the canonical Redfield ratio of 16 (Fig. 13). Moreover, among the different stations, the cluster of productive stations located north of the PF had a significantly lower average N : P ratio (10.5 ± 3.3) than all other clusters (> 11). Indeed the N : P ratio is highly variable in phytoplankton (Geider and La Roche, 2002) and tends to be lower than 16 in nutrient-replete cultures of phytoplankton. Klausmeier et al. (2004) showed that the optimal phytoplankton stoichiometry varied, with N : P < 16 associated with phytoplankton growing exponentially and N : P > 16 at competitive equilibrium. For diatoms, Sarthou et al. (2008) have reported an average ratio of 10 ± 4, based on the review of available literature. In the field, N : P ratios vary also widely (Martiny et al., 2013) and low values have been reported in association to the dominance of diatoms (Arrigo et al., 2002). Our observations of low N : P ratios are consistent with the dominance of diatoms in the KEOPS2 region. The lowest N : P ratio in the most productive region is also confirmed by the temporal evolution of nitrate and phosphate distributions which show a preferential drawdown of phosphate in this region (Blain et al., 2014).

Ecophysiological studies of the effect of iron limitation on phytoplankton elemental ratio has led to different and somewhat contradictory results. The results of Price (2005) with *Thalassiosira weissflogii* suggested that iron limitation leads to a decreased N : P ratio. However Hoffman et al. (2007) working with *Fragilariopsis kerguelensis* and *Chaetoceros dichaeta* did not observe any change in C/N/P ratios in relation to iron limitation. During EIFEX, the initial N : P ratios and their evolution as the bloom developed were very different for two different size classes (Hoffmann et al., 2006). For the microphytoplankton ($> 20\,\mu m$), N : P was < 16 before fertilization and increased as the iron fertilized bloom developed. For nanoplankton ($2\,\mu m$ to $20\,\mu m$) the opposite trend was observed: the initial N : P ratio was close to 16 and decreased in the course of the bloom. In the case of the natural iron fertilization around Kerguelen, we also observed a large variablility between stations. But large changes have also been documented at

BGD
11, 8259–8324, 2014

the seasonal scale. N : P of 17 ± 2 was measured in March (Copin-Montegut and Copin-Montegut, 1978) at stations east of the Kerguelen Islands that were close to the cluster of stations E. All these results suggest that the variability of N : P ratios occurring in response to iron fertilization is ecologically driven. How these changes translated in the N and P elemental composition of sinking particulate matter would certainly deserve further studies.

The C : N ratio was close to the Redfield ratio only at the HNLC station. For all other stations, the C : N ratio was significantly lower but without any difference between the different clusters of stations. This confirms that the C : N ratio is generally not largely affected by iron limitation (Price, 2005; Hoffmann et al., 2007). Low values were previously reported in the Southern Ocean including the Kerguelen region (Copin-Montegut and Copin-Montegut, 1978; Tréguer et al., 1988). This was considered as a general feature of the iron limited Southern Ocean and interpreted as an excess of P accumulation during Fe-limited growth of phytoplankton (Price, 2005). Hoffmann et al. (2006) also observed low C : P ratios in HNLC waters of the Atlantic sector of the Southern Ocean, with only a modest increase in response to iron fertilization. Our results from KEOPS2 also report low C : P ratios in response to iron fertilization. However similarly to what was discussed above for N : P, C : P increased to values close to the Redfield ratio at the end of the season (Copin-Montegut and Copin-Montegut, 1978).

In the Southern Ocean, iron limitation and iron fertilization may favor P accumulation in phytoplankton for different physiological or ecological reasons, leading to N : P and C : P lower than Redfield ratios. However this conclusion based on average values may hind differences especially on temporal scales that are not resolved by the resolution of this data set. Overall, our results also confirm a tendency of a decrease of C : N : P ratios in nutrient-rich high latitude waters highlighted by Martiny et al. (2013) by comparison with warmer oligotrophic or upwelling areas.

BGD
11, 8259–8324, 2014

4.3.4 Seasonal evolution of Si, C and N cycles at the southeast plateau bloom

The KEOPS program provides information on the biogeochemical functioning of the southeastern KP at two different periods of the seasonal cycle: the early spring (October–November 2011 – KEOPS2) and the late summer (January–February 2005 – KEOPS1). Combining the two data sets at station A3 gives us the first opportunity to describe the seasonal evolution of Si, C and N cycles under natural iron fertilization in relation to community composition.

During the KEOPS2 cruise, the first visit at A3 (20 October, A3-1) was characteristic of early bloom conditions. Low biogenic and particulate organic matter concentrations were observed despite high nutrients (Blain et al., 2014) and iron concentrations (Bowie et al., 2014) as well as a low mesozooplankton grazing pressure (Carlotti et al., 2014). Phytoplankton growth was most likely limited by low irradiance levels as expected in winter and early spring (Boyd, 2002). Integrated elemental ratios (over 200 m) were close to the canonical ratios of Redfield et al. (1963) and Brzezinski et al. (1985), reaching values of 0.13 for Si : C, 1.2 for Si : N, 16.9 for Si : P, 9.0 for C : N, 128.7 for C : P and 14.3 for N : P.

At the second visit (November, 16), a large development of diatoms was observed above the KP due to more favorable light conditions. Biogenic silica and particulate organic matter concentrations were at least 2 fold higher than in October (713.3 mmol Si m^{-2} for BSi, 2267 mmol C m^{-2} for POC, 435.9 mmol N m^{-2} for PON, and 29.3 mmol P m^{-2} for POP) and Si production fluxes were among the highest reported so far in the Southern Ocean (47.9 mmol Si m^{-2} d^{-1}; Closset et al., 2014). Si : C and Si : N ratios (respectively 0.31 and 1.6) were higher than Brzezinski's ratios (1985). This could directly result from the high Si : C and Si : N uptake ratios (respectively 0.30 and 1.5) reported by Closset et al. (2014) which were remarkably close to our stock ratios, meaning that it is a characteristic of the species growing in our study area. At this period, the organic carbon produced would be transferred to small zooplankton populations which in turn would feed the large zooplankton population (Henjes et al.,

BGD
11, 8259–8324, 2014

2007). The C budget of Christaki et al. (2014) however, indicates that an overall small fraction of primary production is transferred to higher trophic levels. Added to the low vertical export of C reported by Planchon et al. (2014), both observations are strong arguments of biogenic matter retention in the surface mixed layer at the beginning of the KP bloom.

During the KEOPS1 cruise, the period from 19 January to 12 February corresponded to the last active stage of the productive period. At the start of the cruise, an unusually high level of BSi had already accumulated (2105 mmol Si m^{-2}) in the mixed layer which progressively declined until February (Mosseri et al., 2008). Si : C and Si : N uptake ratios were close to 0.13 and 1. However, the high NO_3^- concentrations in surface waters compared to H_4SiO_4 depletion at the end of the bloom suggested a strong decoupling between the seasonal consumption of these two nutrients. This could be due to differential remineralisation rates between Si and N, as evidenced by elevated concentration of ammonium, and by the ability of diatoms to grow on ammonium as nitrogen source (Mosseri et al., 2008). The system would thus behave as a strong silicon pump favoring Si export to deep waters compared to N. A decoupling between C and N cycles was also hypothesized: high amounts of exported C were reported evidencing a strong biological pump of C (Mosseri et al., 2008; Trull et al., 2008). So, the end of the productive period would be associated to the main event of massive export of biogenic silica and organic matter as proposed by Quéguiner (2013). This feature seems coherent when comparing the most abundant diatom species found in surface waters at the end of the productive period and those found in sediment thanatocoenoses. Indeed, *Eucampia antarctica* and *Chaetoceros* resting spores were the dominant species both in surface waters and in the sediments (Armand et al., 2008; Wilks, 2013) suggesting enhanced export of particulate matter at the end of the productive period.

BGD
11, 8259–8324, 2014

4.4 LSi as tracer of lithogenic matter transport?

All over the study area, LSi concentrations fell in the same range of values previously measured in the Southern Ocean, both in the PFZ (Quéguiner et al., 1997; Quéguiner, 2001; Leblanc et al., 2002) and the POOZ (Quéguiner et al., 1997; Bucciarelli et al., 2001). TNS1 and R stations showed low LSi concentrations typically observed for regions far from continental influence ($< 0.04\ \mu mol\ L^{-1}$; Leblanc et al., 2002). Surprisingly, a local maximum was reported at 500 m at station R, reflecting particulate lithogenic inputs at depth. A similar pattern was found for particulate and dissolved trace metals (Bowie et al., 2014; Quéroué et al., 2014; van der Merwe et al., 2014). In these studies, lateral transport of lithogenic matter from the Leclaire Rise, a large seamount located west of station R, was hypothesized to explain this local maximum.

In contrast to R and TNS1, two regions were characterized by very high LSi concentrations typically reported for regions subjected to continental influence (Bucciarelli et al., 2001): the coastal waters over the entire water column (TEW1 to TEW3) and the reference plateau station A3 near the bottom. For the coastal waters (TEW1 to TEW3), LSi could come from multiple lithogenic sources such as soil erosion, riverine discharges or aeolian inputs (Bucciarelli et al., 2001). At A3, the maximum concentration near the bottom would rather reflect sediment resuspension in the water column. Another striking feature at A3 was the relatively high concentrations from the surface down to 300 m. Two potential sources of lithogenic material could explain these higher concentrations: LSi could come from below due to an elevated vertical mixing or from the extensive shoal around the Heard/Mc Donald Islands by horizontal advection (Blain et al., 2007; Park et al., 2008a). Interestingly, maximum concentrations were found at 400 m for E4W and between 600 and 700 m for the E stations. This could evidence lateral transport of LSi-rich waters coming from the plateau and more likely from the Heard/Mc Donald Islands in the case of E4W. Our results were consistent with the study of Bowie et al. (2014) which reported lithogenic particulate iron coming from the plateau between 400 and 600 m at stations E1, E3 and E5.

BGD
11, 8259–8324, 2014

In the PF area (from TEW7 to TEW8), relatively higher concentrations compared to surrounding waters ($> 0.11\,\mu mol\,L^{-1}$) were observed over the water column. Such a pattern was already reported by previous studies in different sectors of the Southern Ocean (Quéguiner et al., 1997; Bucciarelli et al., 2001). At the southern border of the PFZ in the Atlantic sector, high LSi concentrations were associated to local inputs from atmospheric deposition. By using the NOAA HYSPLIT 1 day and 5 day backward trajectory atmospheric model, no atmospheric inputs were evidenced as suggested by the absence of air masses flowing over the eastern area north of the PF (Quéroué et al., 2014). However, considering that no direct measurements of dust deposition were performed during KEOPS2, the hypothesis of aeolian inputs cannot be completely rejected. In addition, a recent study performed in the Kerguelen region demonstrated that atmospheric deposition fluxes have been underestimated until now (Heimburger et al., 2012). Both eolian inputs and lateral advection of LSi-rich waters could thus explain the relatively higher concentrations between TEW7 and TEW8. LSi-rich waters would probably result from the northwest transport of deep waters from the KP (Zhou et al., 2014) or from the mixture of the advected coastal waters with the subantarctic water (Bucciarelli et al., 2001). The station TNS2, located north of the PF, would also suggest eolian dust deposition coupled with lateral advection of LSi-rich waters by evidencing local LSi maximums at the surface and subsurface.

By comparing particulate iron and other trace metal distribution (Bowie et al., 2014), similar patterns were observed at R, A3 and E stations over the water column. This suggests that LSi would be a good tracer to track lithogenic material inputs (and indirectly iron) from eolian transport, terrestrial erosion as well as sediment resuspension to the water column. All the more so that the Kerguelen Islands are mainly composed of flood basalt, a Si-rich rock (Gautier, 1987). In this study, several potential sources were mentioned to explain the distribution of lithogenic matter all over the study area. The northward transport of lithogenic matter and vertical transport from deep waters enriched in lithogenic materials were expected from the KEOPS1 study (Blain et al., 2007; van Beek et al., 2008; Park et al., 2008a). Furthermore, even if the contribution

BGD
11, 8259–8324, 2014

of atmospheric inputs is still matter of debate (Cassar et al., 2007; Heimburger et al., 2012), dust deposition could play a significant role in supplying lithogenic matter in the Kerguelen region.

5 Conclusions

The distribution of particulate matter and phytoplankton community structure above the natural iron-fertilized Kerguelen region was strongly impacted by the complex mesoscale structure of water masses, generated by the interaction between the KP topography and the Polar Front pathway. In early spring, the eastern side of the KP was characterized by a mosaic of biogeochemical situations that could be divided into five contrasted environments. A productive coastal area was first isolated by a shelf break front from a second area less productive corresponding to a cold water tongue circulating northward and likely limited by light availability. The situation was different in the meander of the PF, where the complex mesoscale activity induced a phytoplankton development delayed by comparison to the KP itself. Two high productive areas were located at the easternmost study area north in the PF and over the southeastern KP where light conditions and nutrients (including iron) availability were favorable to phytoplankton growth. Biogeochemical properties of the eastern flank of the KI supports the idea that the extensive bloom of the southeastern KP was, at least partly, advected northwards.

The comparison between the iron-fertilized productive sites and the iron-limited HNLC area showed that iron stimulated the accumulation of large ($>20\,\mu m$) siliceous particulate matter at the onset of the bloom. Under iron stress, the low Si biomass was mainly associated to mixed, nanoflagellate-dominated, phytoplankton population but Si : C : N : P ratios were unexpectedly close to the typical values for nutrient-replete diatoms, which was likely due to the presence of siliceous detritus from an earlier bloom. In the iron-fertilized areas, we showed a patchy response of particulate matter distribution and stoichiometric ratios but with overall elevated Si : C : N : P. This suggests the

BGD
11, 8259–8324, 2014

presence of heavily silicified diatoms contrary to the classical paradigm of Hutchins and Bruland (1998) and Takeda (1998). The variable and patchy nature of responses in the natural surroundings of the KI calls for cautious consideration in extrapolating the results from artificial iron fertilization experiments.

The seasonal evolution of the bloom over the southeastern KP (A3 station) is characterized by a progressive evolution of the Si : C : N ratios and the phytoplankton community composition probably resulting in different export regimes at the beginning (retention in the ML) and the end of the productive season (massive vertical export). At the onset of the bloom, the weak vertical export, mainly driven by nanoplanktonic size fraction of biogenic silica, could be the result of the fragmentation of particles originating from aborted late winter blooms. Given the high Si : C : N ratios in the surface waters and the expected preferential degradation of organic matter by small zooplankton community in the course of the productive period, the system behaves as a moderate silicon pump in spring. At the end of the bloom, the increasing influence of silicic acid depletion and changes in the phytoplankton community structure result in decreased Si : C and Si : N ratios. Additionally, increased grazing pressure from mesozooplankton leads to a massive export of biogenic silica and carbon organic matter at depth which occurs later in the season (Rembauville et al., 2014). In the natural iron fertilized Kerguelen region, understanding the patchy development of distinct blooms with varying Si : C : N : P composition and the ultimate fate of produced biogenic silica and organic carbon (as in the "silica-sinkers" vs. "carbon-sinkers" hypothesis; Assmy et al., 2013) calls for a finer caracterization of diatoms interspecific contribution to both Si production and C biomass, which can only be adressed by taxonomic studies and cellular labelling (Lasbleiz et al., 2014). As emphasized by Boyd (2013), the concept of functional group tends to fall short when probing its responses to environmental forcings and diatom floristic shifts impact on global biogeochemical cycles needs to be further understood.

Acknowledgements. We thank the captain Bernard Lassiette and crew of the R/V *Marion Dufresne* for their support aboard. We also thank M. Ouhssain from the French SAPIGH analytical platform for pigment sampling and analysis. This work was supported by the French Re-

BGD
11, 8259–8324, 2014

search program of INSU-CNRS LEFE-CYBER ("Les enveloppes fluides et l'environnement" – "Cycles biogéochimiques, environnement et ressources"), the French ANR ("Agence Nationale de la Recherche", SIMI-6 program), the French CNES ("Centre National d'Etudes Spatiales") and the French Polar Institute IPEV (Institut Polaire Paul-Emile Victor).

References

Armand, L. K., Cornet-Barthaux, V., Mosseri, J., and Quéguiner, B.: Late summer diatom biomass and community structure on and around the naturally iron-fertilised Kerguelen Plateau in the Southern Ocean, Deep-Sea Res. Pt. II, 55, 653–676, doi:10.1016/j.dsr2.2007.12.031, 2008.

Armstrong, R. A., Peterson, M. L., Lee, C., and Wakeham, S. G.: Settling velocity spectra and the ballast ratio hypothesis, Deep-Sea Res. Pt. II, 56, 1470–1478, doi:10.1016/j.dsr2.2008.11.032, 2009.

Arrigo, K. R. and Alderkamp, A.-C.: Shedding dynamic light on Fe limitation (DynaLiFe), Deep-Sea Res. Pt. II, 71–76, 1–4, doi:10.1016/j.dsr2.2012.03.004, 2012.

Arrigo, K. R., Dunbar, R. B., Lizotte, M. P., and Robinson, D. H.: Taxon-specific differences in C/P and N/P drawdown for phytoplankton in the Ross Sea, Antarctica, Geophys. Res. Lett., 29, 1938, doi:10.1029/2002gl015277, 2002.

Assmy, P., Smetacek, V., Montresor, M., Klaas, C., Henjes, J., Strass, V. H., Arrieta, J. M., Bathmann, U., Berg, G. M., Breitbarth, E., Cisewski, B., Friedrichs, L., Fuchs, N., Herndl, G. J., Jansen, S., Krägefsky, S., Latasa, M., Peeken, I., Rüttgers, R., Scharek, R., Schüller, S. E., Steigenberger, S., Webb, A., and Wolf-Gladrow, D.: Thick-shelled, grazer-protected diatoms decouple ocean carbon and silicon cycles in the iron-limited Antarctic Circumpolar Current, P. Natl. Acad. Sci. USA, 110, 20633–20638, 2013.

Banse, K.: Should we continue to use the 1 % light depth convention for estimating the compensation depth of phytoplankton for another 70 years?, Limnol. Oceanogr.Bulletin, 13, 49–51, 2004.

Bathmann, U. V., Scharek, R., Klaas, C., Dubischar, C. D., and Smetacek, V.: Spring development of phytoplankton biomass and composition in major water masses of the Atlantic sector of the Southern Ocean, Deep-Sea Res. Pt. II, 44, 51–67, doi:10.1016/S0967-0645(96)00063-X, 1997.

BGD
11, 8259–8324, 2014

Blain, S., Tréguer, P., Belviso, S., Bucciarelli, E., Denis, M., Desabre, S., Fiala, M., Martin Jézéquel, V., Le Fèvre, J., Mayzaud, P., Marty, J.-C., and Razouls, S.: A biogeochemical study of the island mass effect in the context of the iron hypothesis: Kerguelen Islands, Southern Ocean, Deep-Sea Res. Pt. I, 48, 163–187, doi:10.1016/S0967-0637(00)00047-9, 2001.

Blain, S., Queguiner, B., Armand, L., Belviso, S., Bombled, B., Bopp, L., Bowie, A., Brunet, C., Brussaard, C., Carlotti, F., Christaki, U., Corbiere, A., Durand, I., Ebersbach, F., Fuda, J.-L., Garcia, N., Gerringa, L., Griffiths, B., Guigue, C., Guillerm, C., Jacquet, S., Jeandel, C., Laan, P., Lefevre, D., Lo Monaco, C., Malits, A., Mosseri, J., Obernosterer, I., Park, Y.-H., Picheral, M., Pondaven, P., Remenyi, T., Sandroni, V., Sarthou, G., Savoye, N., Scouarnec, L., Souhaut, M., Thuiller, D., Timmermans, K., Trull, T., Uitz, J., van Beek, P., Veldhuis, M., Vincent, D., Viollier, E., Vong, L., and Wagener, T.: Effect of natural iron fertilization on carbon sequestration in the Southern Ocean, Nature, 446, 1070–1074, doi:10.1038/nature05700, 2007.

Blain, S., Oriol, L., Capparos, J., Guéneuguès, A., and Obernosterer, I. (Eds.): Distributions and stoechiometry of dissolved nitrogen and phosphorus in the iron fertilized region near Kerguelen (Southern Ocean), Special Issue, Biogeosciences, this volume, 2014.

Bowie, A. W., van der Merwe, P., Trull, T., Quéroué, F., Fourquez, M., Planchon, F., Sarthou, G., and Blain, S.: Iron budgets for three distinct biogeochemical sites around the Kerguelen plateau (Southern Ocean) during the natural fertilization experiment KEOPS-2, Special Issue, Biogeosciences, this volume, 2014.

Boyd, P. W.: Environmental factors controlling phytoplankton processes in the Southern Ocean, J. Phycol., 38, 844–861, doi:10.1046/j.1529-8817.2002.t01-1-01203.x, 2002.

Boyd, P. W.: Biogeochemistry: iron findings, Nature, 446, 989–991, doi:10.1038/446989a, 2007.

Boyd, P. W.: Diatom traits regulate Southern Ocean silica leakage, P. Natl. Acad. Sci. USA, 110, 20358–20359, doi:10.1073/pnas.1320327110, 2013.

Boyd, P. W., LaRoche, J., Gall, M., Frew, R., and McKay, R. M. L.: Role of iron, light, and silicate in controlling algal biomass in subantarctic waters SE of New Zealand, J. Geophys. Res.-Oceans, 104, 13395–13408, doi:10.1029/1999jc900009, 1999.

Brzezinski, M. A.: The Si : C : N ratio of marine diatoms: interspecific variability and the effect of some environmental variables, J. Phycol., 21, 347–357, 1985.

BGD
11, 8259–8324, 2014

Brzezinski, M. A., Nelson, D. M., Franck, V. M., and Sigmon, D. E.: Silicon dynamics within an intense open-ocean diatom bloom in the Pacific sector of the Southern Ocean, Deep-Sea Res. Pt. II, 48, 3997–4018, doi:10.1016/S0967-0645(01)00078-9, 2001.
Bucciarelli, E., Blain, S., and Tréguer, P.: Iron and manganese in the wake of the Kerguelen Islands (Southern Ocean), Mar. Chem., 73, 21–36, doi:10.1016/S0304-4203(00)00070-0, 2001.
Buesseler, K. O.: The decoupling of production and particulate export in the surface ocean, Global Biogeochem. Cy., 12, 297–310, doi:10.1029/97gb03366, 1998.
Buesseler, K. O., Andrews, J. E., Pike, S. M., and Charette, M. A.: The effects of iron fertilization on carbon sequestration in the Southern Ocean, Science, 304, 414–417, doi:10.1126/science.1086895, 2004.
Cailliau, C., Claustre, H., and Giannino, S.: Chemotaxonomic analysis of phytoplankton distribution in the Indian sector of the Southern Ocean during late austral summer, Oceanol. Acta, 20, 721–732, 1997.
Carlotti, F., Nowaczyk, A., Jouandet, M.-P., Lefèvre, D., and Harmelin, M. (Eds.): Mesozooplankton structure and functioning during the onset of the Kerguelen bloom during KEOP2 survey, Special Issue, Biogeosciences, this volume, 2014.
Cassar, N., Bender, M. L., Barnett, B. A., Fan, S., Moxim, W. J., Levy, H., and B., T.: The Southern Ocean biological response to aeolian iron deposition, Science, 317, 1067–1070, doi:10.1126/science.1144602, 2007.
Cavagna, A. J., Lefèvre, D., Dehairs, F., Elskens, M., Fripiat, F., Closset, I., Lasbleiz, M., Flores-Leive, L., Cardinal, D., Leblanc, K., Fernandez, C., Oriol, L., Blain, S., and Quéguiner, B. (Eds.): Biological productivity regime in the surface waters around the Kerguelen Island in the Southern Ocean – from the use of an integrative approach, Special Issue, Biogeosciences, this volume, 2014.
Christaki, U., Lefèvre, D., Georges, C., Colombet, J., Catala, P., Sime-Ngando, T., Blain, S., and Obernosterer, I. (Eds.): Microbial food web dynamics during spring phytoplankton blooms in the naturally iron-fertilized Kerguelen area (Southern Ocean), Special Issue, Biogeosciences, this volume, 2014.
Claustre, H.: The trophic status of various oceanic provinces as revealed by phytoplankton pigment signatures, Limnol. Oceanogr., 39, 1206–1210, doi:10.4319/lo.1994.39.5.1206, 1994.
Closset, I., Lasbleiz, M., Leblanc, K., Quéguiner, B., Cavagna, A.-J., Elskens, M., Navez, J., and Cardinal, D. (Eds.): Seasonal evolution of net and regenerated silica production around

BGD
11, 8259–8324, 2014

a natural Fe-fertilized area in the Southern Ocean estimated from Si isotopic approaches, Special Issue, Biogeosciences, this volume, 2014.
Copin-Montegut, C. and Copin-Montegut, G.: The chemistry of particulate matter from the south Indian and Antarctic oceans, Deep-Sea Res., 25, 911–931, doi:10.1016/0146-6291(78)90633-1, 1978.
Cullen, J. J.: The deep chlorophyll maximum: comparing vertical profiles of chlorophyll *a*, Can. J. Fish. Aquat. Sci., 39, 791–803, doi:10.1139/f82-108, 1982.
d'Ovidio, F., Zhou, M., Park, Y. H., Nencioli, F., Resplandy, L., Doglioli, A., Petrenko, A., Blain, S., and Queguiner, B.: Guiding biogeochemical campaigns with high resolution altimetry: waiting for the SWOT mission, in: Proceedings of 20 Years of Progress in Radar Altimetry Symposium, Venice, Italy, 2012.
de Baar, H. J. W., Van Leeuwe, M. A., Scharek, R., Goeyens, L., Bakker, K. M. J., and Fritsche, P.: Nutrient anomalies in *Fragilariopsis kerguelensis* blooms, iron deficiency and the nitrate/phosphate ratio (A. C. Redfield) of the Antarctic Ocean, Deep-Sea Res. Pt. II, 44, 229–260, doi:10.1016/S0967-0645(96)00102-6, 1997.
de Baar, H. J. W., Boyd, P., Coale, K., Landry, M., Tsuda, A., Assmy, P., Bakker, D. C., Bozec, Y., Barber, R. T., Brzezinski, M., Buesseler, K., Boyé, M., Croot, P., Gervais, F., Gorbunov, M., Harrison, P., Hiscock, W., Laan, P., Lancelot, C., Law, C., Levasseur, M., Marchetti, A., Millero, F., Nishioka, J., Nojiri, Y., van Oijen, T., Riebesell, U., Rijkenberg, M., Saito, H., Takeda, S., Timmermans, K., Veldhuis, M., Waite, A., and Wong, C.-S.: Synthesis of iron fertilization experiments: from the Iron Age in the Age of Enlightenment, J. Geophys. Res., 110, C09S16, doi:10.1029/2004JC002601, 2005.
Dugdale, R. C., Wilkerson, F. P., and Minas, H. J.: The role of a silicate pump in driving new production, Deep-Sea Res. Pt. I, 42, 697–719, doi:10.1016/0967-0637(95)00015-X, 1995.
Ediger, D., Raine, R., Weeks, A. R., Robinson, I. S., and Sagan, S.: Pigment signatures reveal temporal and regional differences in taxonomic phytoplankton composition off the west coast of Ireland, J. Plankton Res., 23, 893–902, doi:10.1093/plankt/23.8.893, 2001.
Falkowski, P. G., Laws, E. A., Barber, R. T., and Murray, J. W.: Phytoplankton and their role in primary, new, and export production, in: Ocean Biogeochemistry, edited by: Fasham, M. R., Global Change – The IGBP Series, Springer, Berlin Heidelberg, 99–121, 2003.
Firme, G. F., Rue, E. L., Weeks, D. A., Bruland, K. W., and Hutchins, D. A.: Spatial and temporal variability in phytoplankton iron limitation along the California coast and consequences for Si,

BGD
11, 8259–8324, 2014

N, and C biogeochemistry, Global Biogeochem. Cy., 17, 1016, doi:10.1029/2001gb001824, 2003.
Franck, V. M., Brzezinski, M. A., Coale, K. H., and Nelson, D. M.: Iron and silicic acid concentrations regulate Si uptake north and south of the Polar Frontal Zone in the Pacific Sector of the Southern Ocean, Deep-Sea Res. Pt. II, 47, 3315–3338, doi:10.1016/S0967-0645(00)00070-9, 2000.
Froneman, P. W., Pakhomov, E. A., and Balarin, M. G.: Size-fractionated phytoplankton biomass, production and biogenic carbon flux in the eastern Atlantic sector of the Southern Ocean in late austral summer 1997–1998, Deep-Sea Res. Pt. II, 51, 2715–2729, doi:10.1016/j.dsr2.2002.09.001, 2004.
Gall, M. P., Boyd, P. W., Hall, J., Safi, K. A., and Chang, H.: Phytoplankton processes, Part 1: Community structure during the Southern Ocean Iron RElease Experiment (SOIREE), Deep-Sea Res. Pt. II, 48, 2551–2570, doi:10.1016/S0967-0645(01)00008-X, 2001.
Gautier, I.: Les basaltes des îles Kerguelen (Terres Australes et Antarctiques Françaises), Ph.D., Université Paris VI, France, 383 pp., 1987.
Geider, R. and La Roche, J.: Redfield revisited: variability of C : N : P in marine microalgae and its biochemical basis, Eur. J. Phycol., 37, 1–17, doi:10.1017/s0967026201003456, 2002.
Goffart, A., Catalano, G., and Hecq, J. H.: Factors controlling the distribution of diatoms and Phaeocystis in the Ross Sea, J. Marine Syst., 27, 161–175, doi:10.1016/S0924-7963(00)00065-8, 2000.
Hare, C. E., DiTullio, G. R., Trick, C. G., Bruland, S. W. W. W., Rue, E. L., and Hutchins, D. A.: Phytoplankton community structure changes following simulated upwelled iron inputs in the Peru upwelling region, Aquat. Microb. Ecol., 38, 269–282, doi:10.3354/ame038269, 2005.
Hare, C. E., DiTullio, G. R., Riseman, S. F., Crossley, A. C., Popels, L. C., Sedwick, P. N., and Hutchins, D. A.: Effects of changing continuous iron input rates on a Southern Ocean algal assemblage, Deep-Sea Res. Pt. I, 54, 732–746, doi:10.1016/j.dsr.2007.02.001, 2007.
Heimburger, A., Losno, R., Triquet, S., Dulac, F., and Mahowald, N.: Direct measurements of atmospheric iron, cobalt, and aluminum-derived dust deposition at Kerguelen Islands, Global Biogeochem. Cy., 26, GB4016, doi:10.1029/2012gb004301, 2012.
Henjes, J., Assmy, P., Klaas, C., Verity, P., and Smetacek, V.: Response of microzooplankton (protists and small copepods) to an iron-induced phytoplankton bloom in the Southern Ocean (EisenEx), Deep-Sea Res. Pt. I, 54, 363–384, doi:10.1016/j.dsr.2006.12.004, 2007.

BGD
11, 8259–8324, 2014

Hoffmann, L. J., Peeken, I., Lochte, K., Assmy, P., and Veldhuis, M.: Different reactions of Southern Ocean phytoplankton size classes to iron fertilization, Limnol. Oceanogr., 51, 1217–1229, doi:10.4319/lo.2006.51.3.1217, 2006.
Hoffmann, L. J., Peeken, I., and Lochte, K.: Effects of iron on the elemental stoichiometry during EIFEX and in the diatoms *Fragilariopsis kerguelensis* and *Chaetoceros dichaeta*, Biogeosciences, 4, 569–579, doi:10.5194/bg-4-569-2007, 2007.
Howard, A. G., Coxhead, A. J., Potter, I. A., and Watt, A. P.: Determination of dissolved aluminium by the micelle-enhanced fluorescence of its lumogallion complex, Analyst, 111, 1379–1382, doi:10.1039/an9861101379, 1986.
Hutchins, D. A. and Bruland, K. W.: Iron-limited diatom growth and Si:N uptake ratios in a coastal upwelling regime, Nature, 393, 561–564, doi:10.1038/31203, 1998.
Hydes, D. J. and Liss, P. S.: Fluorimetric method for the determination of low concentrations of dissolved aluminium in natural waters, Analyst, 101, 922–931, doi:10.1039/an9760100922, 1976.
Jacquet, S. H. M., Dehairs, F., Cavagna, A.-J., Planchon, F., Monin, L., and André, L. (Eds.): Early season mesopelagic carbon remineralization and transfer efficiency in the naturally iron-fertilized Kerguelen area, Special Issue, Biogeosciences, this volume, 2014.
Johnsen, G. and Sakshaug, E.: Bio-optical characteristics and photoadaptive responses in the toxic and bloom-forming dinoflagellates *Gyrodinium aureolum*, *Gymnodinium galatheanum*, and two strains of *Prorocentrum minimum*, J. Phycol., 29, 627–642, doi:10.1111/j.0022-3646.1993.00627.x, 1993.
Jouandet, M. P., Blain, S., Metzl, N., Brunet, C., Trull, T. W., and Obernosterer, I.: A seasonal carbon budget for a naturally iron-fertilized bloom over the Kerguelen Plateau in the Southern Ocean, Deep-Sea Res. Pt. II, 55, 856–867, doi:10.1016/j.dsr2.2007.12.037, 2008.
Klausmeier, C. A., Litchman, E., and Levin, S. A.: Phytoplankton growth and stoichiometry under multiple nutrient limitation, Limnol. Oceanogr., 49, 1463–1470, doi:10.4319/lo.2004.49.4_part_2.1463, 2004.
Kopczyñska, E. E., Fiala, M., and Jeandel, C.: Annual and interannual variability in phytoplankton at a permanent station off Kerguelen Islands, Southern Ocean, Polar Biol., 20, 342–351, doi:10.1007/s003000050312, 1998.
Lance, V. P., Hiscock, M. R., Hilting, A. K., Stuebe, D. A., Bidigare, R. R., Smith Jr., W. O., and Barber, R. T.: Primary productivity, differential size fraction and pigment composition

BGD
11, 8259–8324, 2014

responses in two Southern Ocean in situ iron enrichments, Deep-Sea Res. Pt. I, 54, 747–773, doi:10.1016/j.dsr.2007.02.008, 2007.
Lancelot, C., Hannon, E., Becquevort, S., Veth, C., and de Baar, H. J. W.: Modeling phytoplankton blooms and carbon export production in the Southern Ocean: dominant controls by light and iron in the Atlantic sector in Austral spring 1992, Deep-Sea Res. Pt. I, 47, 1621–1662, doi:10.1016/S0967-0637(00)00005-4, 2000.
Laurenceau, E. C., Trull, T. W., Davis, D. M., Bray, S. G., Doran, J., Planchon, F., Carlotti, F., Jouandet, M.-P., Cavagna, A.-J., Waite, A. M., and Blain, S. (Eds.): Importance of ecosystem structure to carbon export: insights from free-drifting sediment trap deployments in naturally iron-fertilised waters near the Kerguelen plateau, Special Issue, Biogeosciences, this volume, 2014.
Leblanc, K., Quéguiner, B., Fiala, M., Blain, S., Morvan, J., and Corvaisier, R.: Particulate biogenic silica and carbon production rates and particulate matter distribution in the Indian sector of the Subantarctic Ocean, Deep-Sea Res. Pt. II, 49, 3189–3206, doi:10.1016/S0967-0645(02)00078-4, 2002.
Legendre, L. and Le Fèvre, J.: Hydrodynamical singularities as controls of recycled versus export production in oceans in: Geological Journal, Productivity of the Oceans: Present and Past, 63rd edn., edited by: Berger, W. H., Smetacek, V. S., and Wefer, G., Wiley, 49–63, 1989.
Lévy, M., Klein, P., and Treguier, A.-M.: Impact of sub-mesoscale physics on production and subduction of phytoplankton in an oligotrophic regime, J. Mar. Res., 59, 535–565, 2001.
Margalef, R.: Ecological correlations and the relationship between primary productivity and community structure, in: Memorie dell'Istituto Italiano di Idrobiologia, 355–364, 1965.
Marra, J. F., Lance, V. P., Vaillancourt, R. D., and Hargreaves, B. R.: Resolving the ocean's euphotic zone, Deep-Sea Res. Pt. I, 83, 45–50, doi:10.1016/j.dsr.2013.09.005, 2014.
Martin, J. H.: Glacial-interglacial CO_2 change: the iron hypothesis, Paleoceanography, 5, 1–13, doi:10.1029/PA005i001p00001, 1990.
Martin, J. H., Gordon, R. M., and Fitzwater, S. E.: The case for iron, Limnol. Oceanogr., 36, 1793–1802, 1991.
Martiny, A. C., Pham, C. T. A., Primeau, F. W., Vrugt, J. A., Moore, J. K., Levin, S. A., and Lomas, M. W.: Strong latitudinal patterns in the elemental ratios of marine plankton and organic matter, Nat. Geosci., 6, 279–283, doi:10.1038/ngeo1757, 2013.

BGD
11, 8259–8324, 2014

Matsumoto, K., Sarmiento, J. L., and Brzezinski, M. A.: Silicic acid leakage from the Southern Ocean: a possible explanation for glacial atmospheric pCO_2, Global Biogeochem. Cy., 16, 3, doi:10.1029/2001gb001442, 2002.

Moore, C. M., Hickman, A. E., Poulton, A. J., Seeyave, S., and Lucas, M. I.: Iron-light interactions during the CROZet natural iron bloom and EXport experiment (CROZEX): taxonomic responses and elemental stoichiometry, Deep-Sea Res. Pt. II, 54, 2066–2084, doi:10.1016/j.dsr2.2007.06.015, 2007.

Morris, P. J. and Charette, M. A.: A synthesis of upper ocean carbon and dissolved iron budgets for Southern Ocean natural iron fertilisation studies, Deep-Sea Res. Pt. II, 90, 147–157, doi:10.1016/j.dsr2.2013.02.001, 2013.

Mosseri, J., Quéguiner, B., Armand, L., and Cornet-Barthaux, V.: Impact of iron on silicon utilization by diatoms in the Southern Ocean: a case study of Si/N cycle decoupling in a naturally iron-enriched area, Deep-Sea Res. Pt. II, 55, 801–819, doi:10.1016/j.dsr2.2007.12.003, 2008.

Nelson, D. M., Tréguer, P., Brzezinski, M. A., Leynaert, A., and Quéguiner, B.: Production and dissolution of biogenic silica in the ocean: revised global estimates, comparison with regional data and relationship to biogenic sedimentation, Global Biogeochem. Cy., 9, 359–372, doi:10.1029/95gb01070, 1995.

Park, Y.-H., and Gamberoni, L.: Cross-frontal exchange of Antarctic Intermediate Water and Antarctic Bottom Water in the Crozet Basin, Deep-Sea Res. Pt. II, 44, 963–986, doi:10.1016/S0967-0645(97)00004-0, 1997.

Park, Y.-H., Fuda, J.-L., Durand, I., and Naveira Garabato, A. C.: Internal tides and vertical mixing over the Kerguelen Plateau, Deep-Sea Res. Pt. II, 55, 582–593, doi:10.1016/j.dsr2.2007.12.027, 2008a.

Park, Y.-H., Roquet, F., Durand, I., and Fuda, J.-L.: Large-scale circulation over and around the Northern Kerguelen Plateau, Deep-Sea Res. Pt. II, 55, 566–581, doi:10.1016/j.dsr2.2007.12.030, 2008b.

Park, Y.-H., Durand, I., Kestenare, E., Rougier, G., Zhou, M., d'Ovidio, F., and Lee, J.-H. (Eds.): Polar Front around Kerguelen: an up-to-date determination and associated circulation of subsurface waters, Special Issue, Biogeosciences, this volume, 2014.

Peeken, I.: Photosynthetic pigment fingerprints as indicators of phytoplankton biomass and development in different water masses of the Southern Ocean during austral spring, Deep-Sea Res. Pt. II, 44, 261–282, doi:10.1016/S0967-0645(96)00077-X, 1997.

BGD
11, 8259–8324, 2014

Planchon, F., Ballas, D., Cavagna, A.-J., van der Merwe, P., Bowie, A. W., Trull, T., Laurenceau, E. C., Davies, D. M., and Dehairs, F.: Carbon export in the naturally iron-fertilized Kerguelen area of the Southern Ocean using ^{234}Th based approach, Special Issue, Biogeosciences, this volume, 2014.

Pollard, R. T., Salter, I., Sanders, R. J., Lucas, M. I., Moore, C. M., Mills, R. A., Statham, P. J., Allen, J. T., Baker, A. R., Bakker, D. C. E., Charette, M. A., Fielding, S., Fones, G. R., French, M., Hickman, A. E., Holland, R. J., Hughes, J. A., Jickells, T. D., Lampitt, R. S., Morris, P. J., Nedelec, F. H., Nielsdottir, M., Planquette, H., Popova, E. E., Poulton, A. J., Read, J. F., Seeyave, S., Smith, T., Stinchcombe, M., Taylor, S., Thomalla, S., Venables, H. J., Williamson, R., and Zubkov, M. V.: Southern Ocean deep-water carbon export enhanced by natural iron fertilization, Nature, 457, 577–580, doi:10.1038/nature07716, 2009.

Price, N. M.: The elemental stoichiometry and composition of an iron-limited diatom, Limnol. Oceanogr., 50, 1159–1171, doi:10.4319/lo.2005.50.4.1159, 2005.

Pujo-Pay, M. and Raimbault, P.: Improvement of the wet-oxidation procedure for simultaneous determination of particulate organic nitrogen and phosphorus collected on filters, Mar. Ecol.-Prog. Ser., 105, 203–207, 1994.

Quéguiner, B.: Biogenic silica production in the Australian sector of the Subantarctic Zone of the Southern Ocean in late summer 1998, J. Geophys. Res.-Oceans, 106, 31627–31636, doi:10.1029/2000jc000249, 2001.

Quéguiner, B.: Iron fertilization and the structure of planktonic communities in high nutrient regions of the Southern Ocean, Deep-Sea Res. Pt. II, 90, 43–54, doi:10.1016/j.dsr2.2012.07.024, 2013.

Quéguiner, B. and Brzezinski, M. A.: Biogenic silica production rates and particulate organic matter distribution in the Atlantic sector of the Southern Ocean during austral spring 1992, Deep-Sea Res. Pt. II, 49, 1765–1786, doi:10.1016/S0967-0645(02)00011-5, 2002.

Quéguiner, B., Tréguer, P., Peeken, I., and Scharek, R.: Biogeochemical dynamics and the silicon cycle in the Atlantic sector of the Southern Ocean during austral spring 1992, Deep-Sea Res. Pt. II, 44, 69–89, doi:10.1016/S0967-0645(96)00066-5, 1997.

Quéroué, F., Sarthou, G., Chever, F., Van der Merwe, P., Lannuzel, D., Townsend, A., Bucciarelli, E., Planquette, H., Cheize, M., Blain, S., d'Ovidio, F., and Bowie, A. (Eds.): A new study of natural Fe fertilization processes in the vicinity of the Kerguelen Islands (KEOPS2 experiment), Special Issue, Biogeosciences, this volume, 2014.

BGD
11, 8259–8324, 2014

Ragueneau, O., Savoye, N., Del Amo, Y., Cotten, J., Tardiveau, B., and Leynaert, A.: A new method for the measurement of biogenic silica in suspended matter of coastal waters: using Si : Al ratios to correct for the mineral interference, Cont. Shelf. Res., 25, 697–710, doi:10.1016/j.csr.2004.09.017, 2005.

Ras, J., Claustre, H., and Uitz, J.: Spatial variability of phytoplankton pigment distributions in the Subtropical South Pacific Ocean: comparison between in situ and predicted data, Biogeosciences, 5, 353–369, doi:10.5194/bg-5-353-2008, 2008.

Read, J. F., Pollard, R. T., and Allen, J. T.: Sub-mesoscale structure and the development of an eddy in the Subantarctic Front north of the Crozet Islands, Deep-Sea Res. Pt. II, 54, 1930–1948, doi:10.1016/j.dsr2.2007.06.013, 2007.

Redfield, A. C., Ketchum, B. H., and Richards, F. A.: The influence of organisms on the composition of sea water, in: The Sea, edited by: Hill, M. N., Wiley-Interscience, New York, 2677 pp., 1963.

Sarmiento, J. L., Gruber, N., Brzezinski, M. A., and Dunne, J. P.: High-latitude controls of thermocline nutrients and low latitude biological productivity, Nature, 427, 56–60, doi:10.1038/nature02127, 2004.

Sarthou, G., Vincent, D., Christaki, U., Obernosterer, I., Timmermans, K. R., and Brussaard, C. P. D.: The fate of biogenic iron during a phytoplankton bloom induced by natural fertilisation: Impact of copepod grazing, Deep-Sea Res. Pt. II, 55, 734–751, doi:10.1016/j.dsr2.2007.12.033, 2008.

Sarthou, G., Chever, F., Quéroué, F., Bowie, A. R., van der Merwe, P., Cheize, M., Sirois, M., and Bucciarelli, E. (Eds.): Fe-Cu impact in incubation experiments of natural plankton communities and Fe- and Cu-binding ligand production at the vicinity of the Kerguelen Islands, Southern Ocean, Special Issue, Biogeosciences, this volume, 2014.

Schlüter, M. and Rickert, D.: Effect of pH on the measurement of biogenic silica, Mar. Chem., 63, 81–92, doi:10.1016/S0304-4203(98)00052-8, 1998.

Smetacek, V., Klaas, C., Strass, V. H., Assmy, P., Montresor, M., Cisewski, B., Savoye, N., Webb, A., d'Ovidio, F., Arrieta, J. M., Bathmann, U., Bellerby, R., Berg, G. M., Croot, P., Gonzalez, S., Henjes, J., Herndl, G. J., Hoffmann, L. J., Leach, H., Losch, M., Mills, M. M., Neill, C., Peeken, I., Rottgers, R., Sachs, O., Sauter, E., Schmidt, M. M., Schwarz, J., Terbruggen, A., and Wolf-Gladrow, D.: Deep carbon export from a Southern Ocean iron-fertilized diatom bloom, Nature, 487, 313–319, doi:10.1038/nature11229, 2012.

BGD
11, 8259–8324, 2014

Strickland, J. D. H. and Parsons, T. R.: A Practical Handbook of Seawater Analysis, 2nd edn., Fisheries Research Board of Canada, Ottawa, Canada, 207–226, 1972.
Sunda, W. G. and Huntsman, S. A.: Interrelated influence of iron, light and cell size on marine phytoplankton growth, Nature, 390, 389–392, doi:10.1038/37093, 1997.
Takeda, S.: Influence of iron availability on nutrient consumption ratio of diatoms in oceanic waters, Nature, 393, 774–777, doi:10.1038/31674, 1998.
Tarling, G. A., Ward, P., Atkinson, A., Collins, M. A., and Murphy, E. J.: DISCOVERY 2010: spatial and temporal variability in a dynamic polar ecosystem, Deep-Sea Res. Pt. II, 59–60, 1–13, doi:10.1016/j.dsr2.2011.10.001, 2012.
Tester, P. A., Geesey, M. E., Guo, C., Paerl, H. W., and Millie, D.: Evaluating phytoplankton dynamics in the Newport River Estuary (North Carolina, USA) by HPLC-derived pigment profiles, Mar. Ecol.-Prog. Ser., 124, 237–245, doi:10.3354/meps124237, 1995.
Timmermans, K. R., Gerringa, L. J., Baar, H. J. D., van der Wagt, B., Veldhuis, M. J., Jong, J. T. d., Croot, P. L., and Boye, M.: Growth rates and small Southern Ocean diatoms in relation to availability of iron in natural seawater, Limnol. Oceanogr., 46, 260–266, doi:10.4319/lo.2001.46.2.0260, 2001.
Timmermans, K. R., Veldhuis, M. J. W., Laan, P., and Brussaard, C. P. D.: Probing natural iron fertilization near the Kerguelen (Southern Ocean) using natural phytoplankton assemblages and diatom cultures, Deep-Sea Res. Pt. II, 55, 693–705, doi:10.1016/j.dsr2.2007.12.008, 2008.
Tréguer, P., Gueneley, S., and Kamatani, A.: Biogenic silica and particulate organic matter from the indian sector of the Southern Ocean, Mar. Chem., 23, 167–180, doi:10.1016/0304-4203(88)90030-8, 1988.
Trull, T. W., Davies, D., and Casciotti, K.: Insights into nutrient assimilation and export in naturally iron-fertilized waters of the Southern Ocean from nitrogen, carbon and oxygen isotopes, Deep-Sea Res. Pt. II, 55, 820–840, doi:10.1016/j.dsr2.2007.12.035, 2008.
Uitz, J., Claustre, H., Morel, A., and Hooker, S. B.: Vertical distribution of phytoplankton communities in open ocean: an assessment based on surface chlorophyll, J. Geophys. Res.-Oceans, 111, C08005, doi:10.1029/2005jc003207, 2006.
Uitz, J., Claustre, H., Griffiths, F. B., Ras, J., Garcia, N., and Sandroni, V.: A phytoplankton class-specific primary production model applied to the Kerguelen Islands region (Southern Ocean), Deep-Sea Res. Pt. I, 56, 541–560, doi:10.1016/j.dsr.2008.11.006, 2009.

BGD
11, 8259–8324, 2014

van Beek, P., Bourquin, M., Reyss, J. L., Souhaut, M., Charette, M. A., and Jeandel, C.: Radium isotopes to investigate the water mass pathways on the Kerguelen Plateau (Southern Ocean), Deep-Sea Res. Pt. II, 55, 622–637, doi:10.1016/j.dsr2.2007.12.025, 2008.

van der Merwe, P., Bowie, A., Quéroué, F., Sarthou, G., Chever, F., Trull, T., Armand, L., Davis, D., Dehairs, F., Townsend, A. R., and Blain, S. (Eds.): Sourcing the iron in the naturally fertilised bloom around the Kerguelen plateau: particulate trace metal dynamics, Special Issue, Biogeosciences, this volume, 2014.

Van Heukelem, L. and Thomas, C. S.: Computer-assisted high-performance liquid chromatography method development with applications to the isolation and analysis of phytoplankton pigments, 1, Elsevier, Amsterdam, Pays-bas, 2001.

Vidussi, F., Claustre, H., Manca, B. B., Luchetta, A., and Marty, J.-C.: Phytoplankton pigment distribution in relation to upper thermocline circulation in the eastern Mediterranean Sea during winter, J. Geophys. Res.-Oceans, 106, 19939–19956, doi:10.1029/1999jc000308, 2001.

Wilks, J. V.: Diatom distribution and community composition variability on the seafloor in a naturally iron fertilised region of the Southern Ocean, Unpublished Honours Thesis, Macquarie University, North Ryde, Australia, 74 pp., 2013.

Wright, S. W. and Jeffrey, S. W.: Fucoxanthin pigment markers of marine phytoplankton analysed by HPLC and HPTLC, Mar. Ecol.-Prog. Ser., 38, 259–266, doi:10.3354/meps038259, 1987.

Wright, S. W. and van den Enden, R. L.: Phytoplankton community structure and stocks in the East Antarctic marginal ice zone (BROKE survey, January–March 1996) determined by CHEMTAX analysis of HPLC pigment signatures, Deep-Sea Res. Pt. II, 47, 2363–2400, doi:10.1016/S0967-0645(00)00029-1, 2000.

Zhou, M., Zhu, Y., Dorland, R. D., and Measures, C. I.: Dynamics of the current system in the southern Drake Passage, Deep-Sea Res. Pt. I, 57, 1039–1048, doi:10.1016/j.dsr.2010.05.012, 2010.

Zhou, M., Zhu, Y., Measures, C. I., Hatta, M., Charette, M. A., Gille, S. T., Frants, M., Jiang, M., and Greg Mitchell, B.: Winter mesoscale circulation on the shelf slope region of the southern Drake Passage, Deep-Sea Res. Pt. II, 90, 4–14, doi:10.1016/j.dsr2.2013.03.041, 2013.

Zhou, M., Zhu, Y., d'Ovidio, F., Park, Y.-H., Durand, I., Kestenare, E., Sanial, V., van Beek, P., Quéguiner, B., Carlotti, F., and Blain, S.: Surface currents and upwelling in Kerguelen Plateau regions, Special Issue, Biogeosciences, this volume, 2014.

BGD
11, 8259–8324, 2014

Table 1. Integrated concentrations in BSi, POC, PON and POP (in mmol m^{-2}) over 200 m depth (except for the coastal station TEW2, integrated over 70 m) North and South of the Polar Front.

	Integrated concentrations (mmol m^{-2})	
	North of the PF (Stations TEW2, TEW3, TNS1, TNS2)	South of the PF (Stations TEW4 to TEW6, TNS3 to TNS10, A3-1)
Σ PSi	33.5–141.0	240.0–460.3
Σ POC	456.9–629.6	562.9–1,164.2
Σ PON	83.1–144.9	143.5–250.3
Σ POP	5.7–10.1	8.7–18.9

BGD
11, 8259–8324, 2014

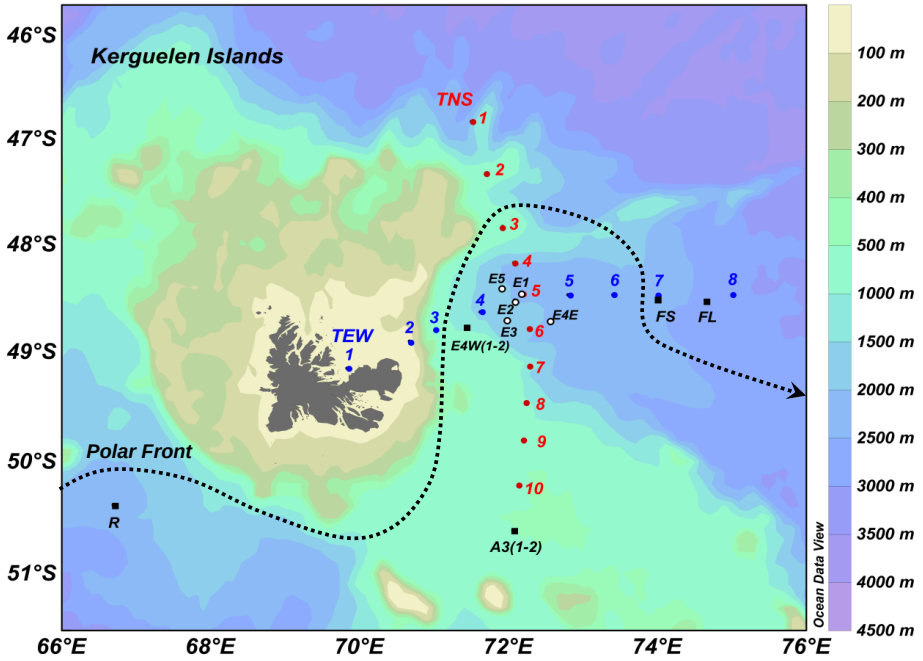

Figure 1. Location of the sampling stations. Transects from North to South (TNS) and from West to the East (TEW) are indicated in red and blue respectively. The blank filled circles correspond to a time-series of a recirculation system. The dotted line represents the approximate location of the southern branch of the Polar Front.

BGD
11, 8259–8324, 2014

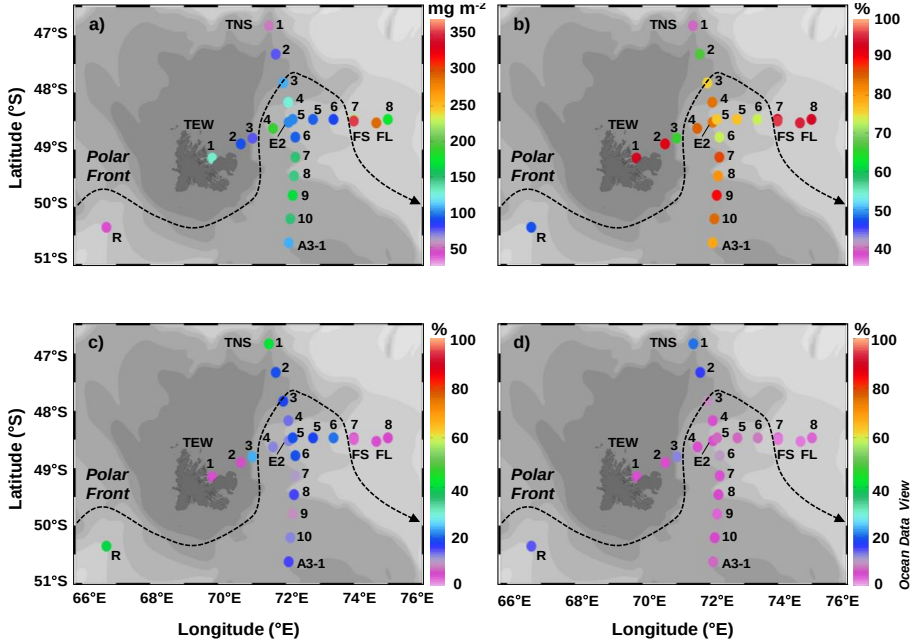

Figure 2. Distribution of depth-integrated total chlorophyll *a* **(a)** and contribution of micro- **(b)**, nano- **(c)**, picophytoplankton **(d)** communities to total biomass. Vertical integrations were made from the surface to 200 m except for the coastal stations TEW1 and TEW2 where data were integrated down to 70 m. The TNS transect (comprising A3-1) was sampled from the 20 to the 23 October, while the TEW transect (comprising E2) was sampled between the 31 October and 2 November. Station R was sampled between the two transects on the 25 October, while stations F were sampled after the two transects, on the 6 November (FL), and the 8 November (FS). The dashed line represents the Polar Front trajectory.

BGD
11, 8259–8324, 2014

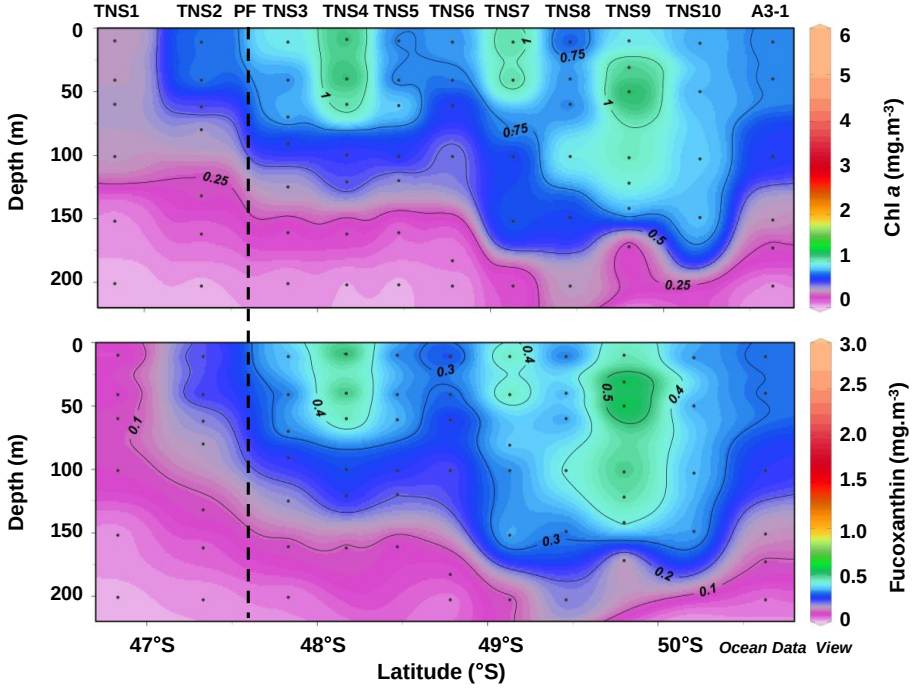

Figure 3. Vertical distribution of total chlorophyll *a* (Chl *a*) and fucoxanthin concentrations along the TNS transect. The dashed line represents the approximate location of the southern branch of the Polar Front (PF).

BGD
11, 8259–8324, 2014

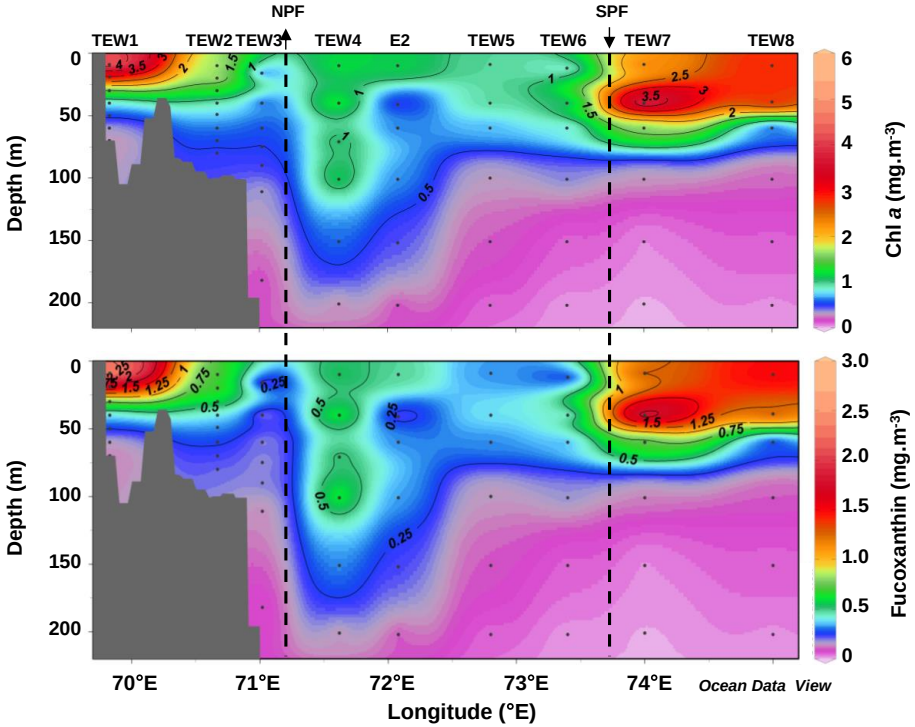

Figure 4. Vertical distribution of total chlorophyll *a* (Chl *a*) and fucoxanthin concentrations along the TEW transect. The dashed lines represent the approximate location of the southern branch of the Polar Front going to the north (NPF) and to the south (SPF).

BGD
11, 8259–8324, 2014

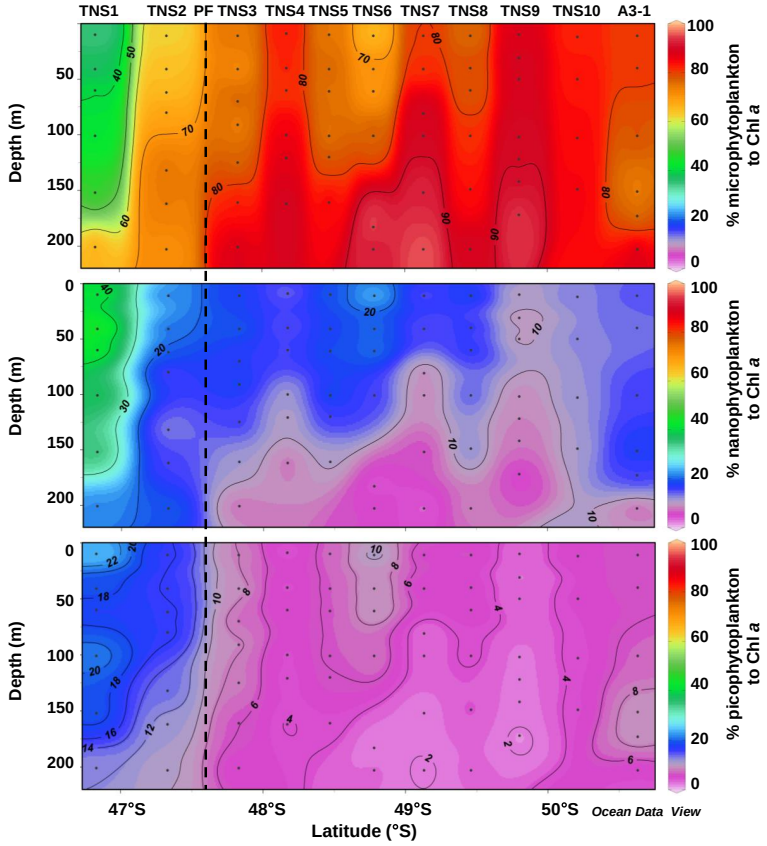

Figure 5. Vertical distribution of micro-, nano- and picophytoplankton community contributions to total biomass along the TNS transect. The dashed line represents the approximate location of the southern branch of the Polar Front (PF).

BGD
11, 8259–8324, 2014

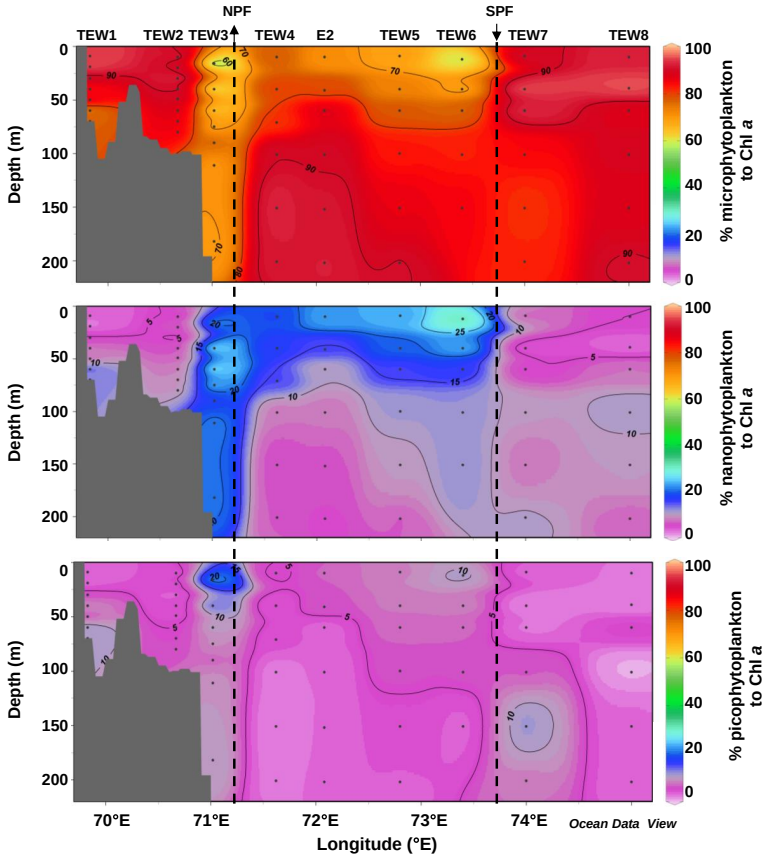

Figure 6. Vertical distribution of micro-, nano- and picophytoplankton community contributions to total biomass along the TEW transect. The dashed lines represent the approximate location of the southern branch of the Polar Front going to the North (NPF) and to the South (SPF).

BGD
11, 8259–8324, 2014

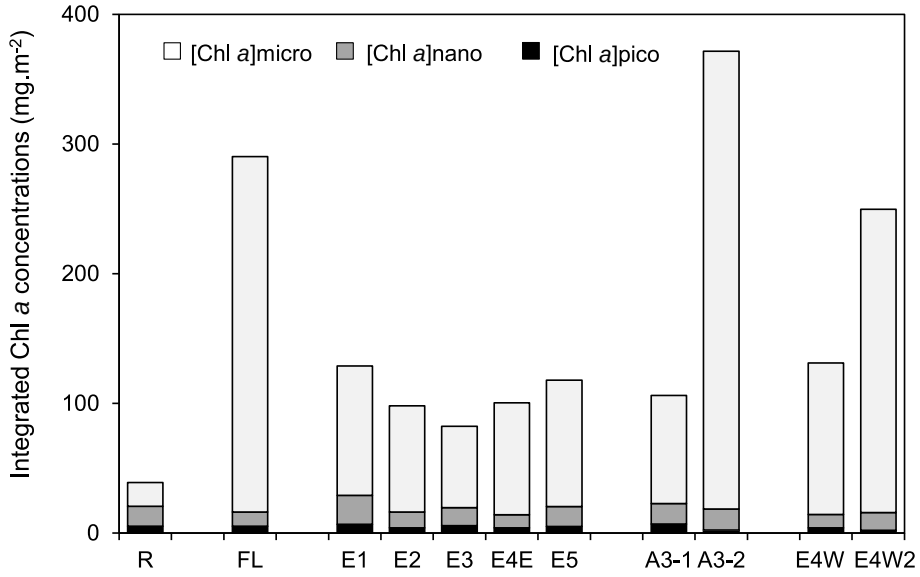

Figure 7. Temporal evolution of Chl *a* concentrations associated with micro- ([Chl *a*]micro), nano- ([Chl *a*]nano) and picophytoplankton ([Chl *a*]pico) within 200 m at the complex system of recirculation (five visits chronologically numerated: E1 (29 October), E2 (1 November), E3 (3 November), E4E (13 November), E5 (19 November)), at the plateau reference station A3 (two visits: A3-1 (20 October) and A3-2 (16 November)) and at station E4W (two visits: E4W (12 November) and E4W2 (18 November)). The station FL (integrated within 150 m) and the HNLC reference station R are presented for comparison.

BGD
11, 8259–8324, 2014

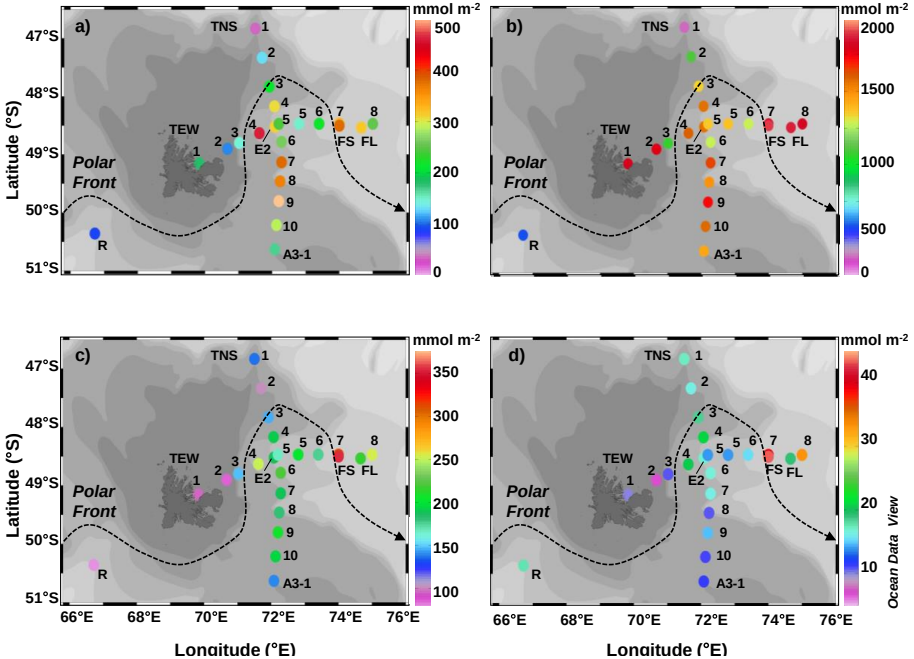

Figure 8. Distribution of biogenic silica **(a)**, particulate organic carbon **(b)**, nitrogen **(c)** and phosphorus **(d)** (same vertical integrations and legends as Fig. 2).

BGD
11, 8259–8324, 2014

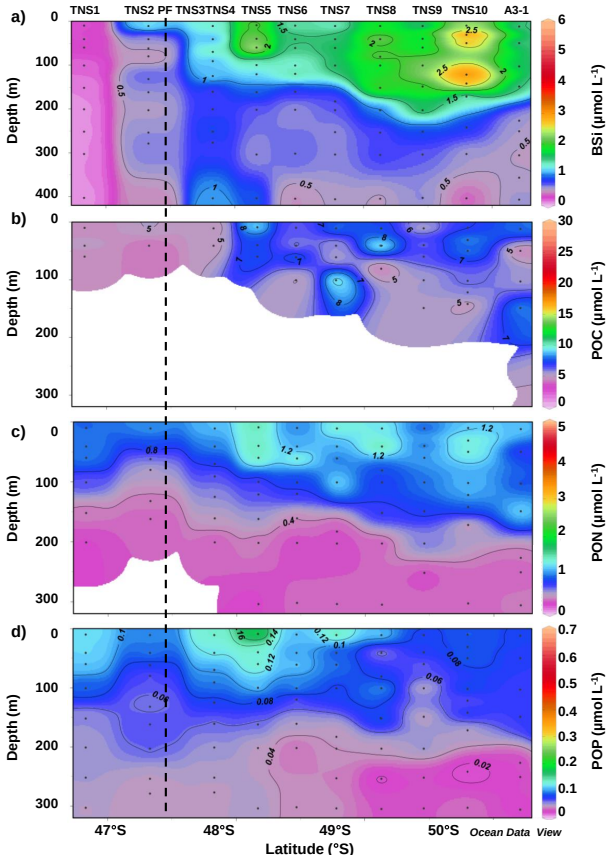

Figure 9. Vertical distributions of BSi **(a)**, POC **(b)**, PON **(c)**, POP **(d)** concentrations along the TNS transect. The dashed line represents the approximate location of the southern branch of the Polar Front (PF).

BGD
11, 8259–8324, 2014

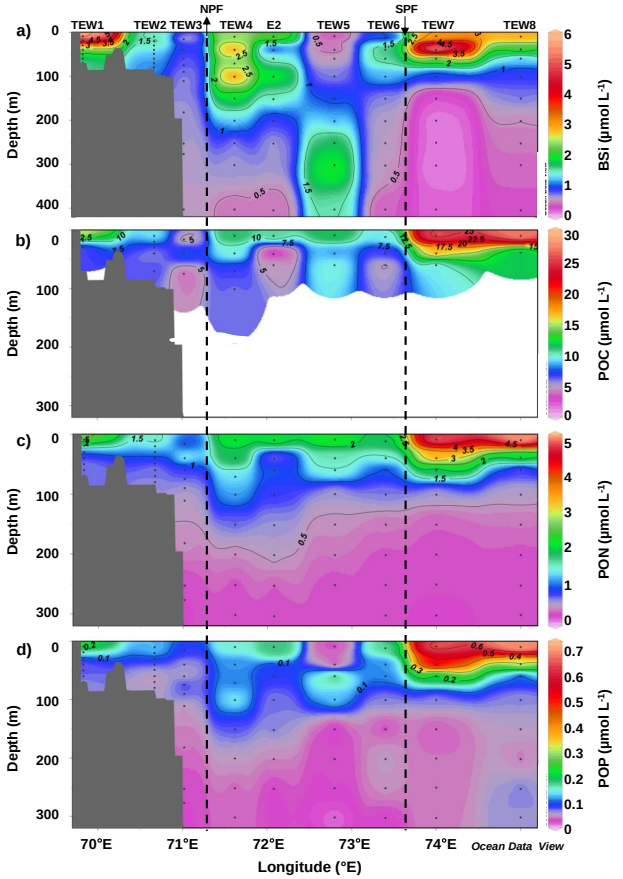

Figure 10. Vertical distributions of BSi **(a)**, POC **(b)**, PON **(c)**, POP **(d)** concentrations along the TEW transect. The dashed lines represent the approximate location of the southern branch of the Polar Front going to the North (NPF) and to the South (SPF).

BGD
11, 8259–8324, 2014

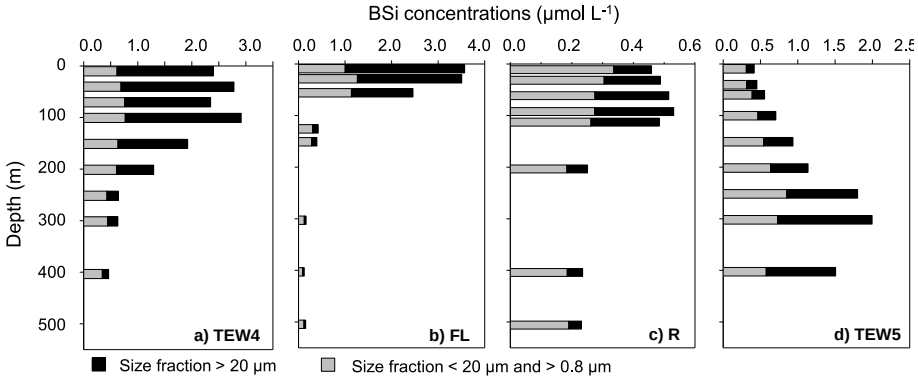

Figure 11. Vertical profiles of BSi concentrations for two size fractions (> 20 µm in black and between 0.8 and 20 µm in grey) at four typical stations: the productive stations TEW4 **(a)** and FL **(b)** and the non-productive stations R **(c)** and TEW5 **(d)**.

BGD
11, 8259–8324, 2014

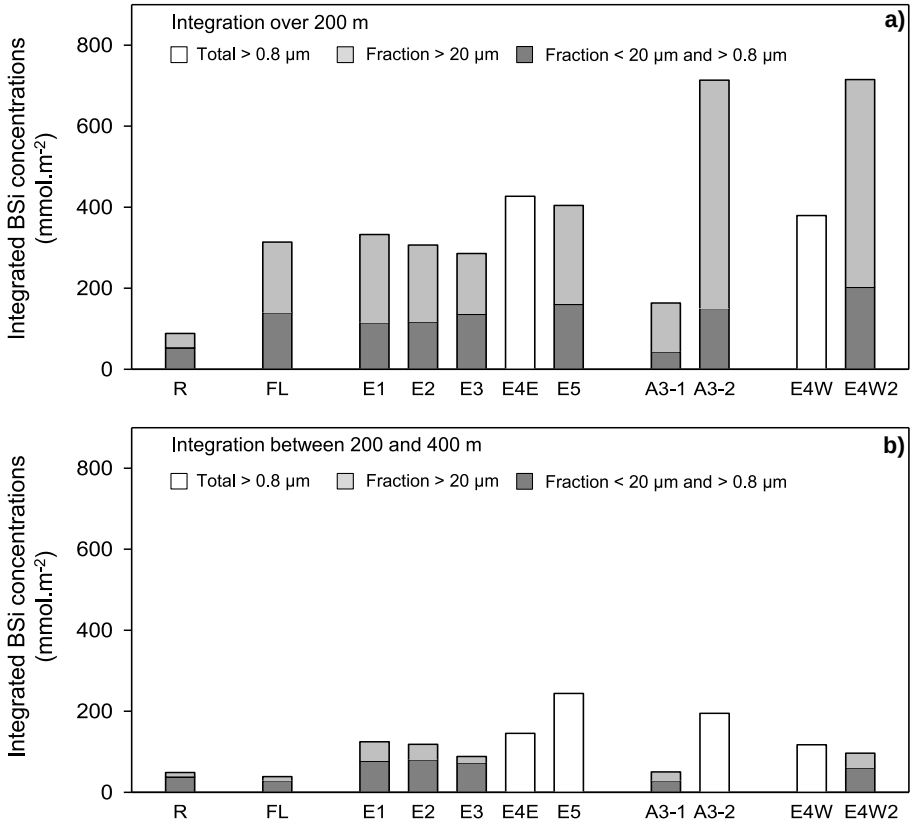

Figure 12. Temporal evolution of BSi concentrations within 200 m **(a)** (except for A3-2 where data were integrated down to 160 m) and between 200 and 400 **(b)** for three size fractions (> 0.8 µm, between 0.8 and 20 µm and > 20 µm) at the complex system of recirculation, at the plateau reference station A3, at station E4W (stations legend as in Fig. 7). The station FL and the HNLC reference station R are presented for comparison.

BGD
11, 8259–8324, 2014

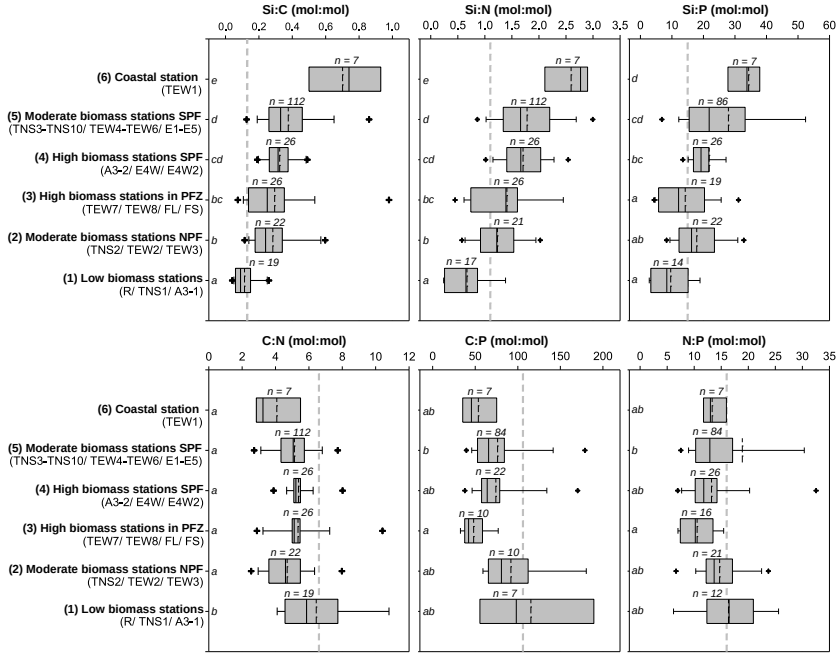

Figure 13. Box plots of the Si : C, Si : N, Si : P, C : N, C : P and N : P molar ratios within 200 m (except for TEW1 and TEW2 where data were restricted within 70 m) for 6 clusters of stations located in the Polar Front Zone (PFZ), north (NPF) and south of the Polar Front (SPF). The length of the box corresponds to the distance between the 5 and the 95 percentiles. The plain line and the dashed line inside the box represent the median and the mean respectively. The vertical lines extend to the minimum and maximum values of the cluster. The cross symbols correspond to outliers and "*n*" is the number of values in each cluster. The grey dashed lines represent the typical values of Si : C (0.13), Si : N (1.1) and Si : P (15) for nutrient-replete diatoms reported by Brzezinski (1985) and the typical values of C : N (6.6), C : P (106) and N : P (16) reported by Redfield et al. (1963). The clusters of which medians are not statistically different are indicated by the same letter (Mann–Whitney *U* test, $p > 0.05$).

BGD
11, 8259–8324, 2014

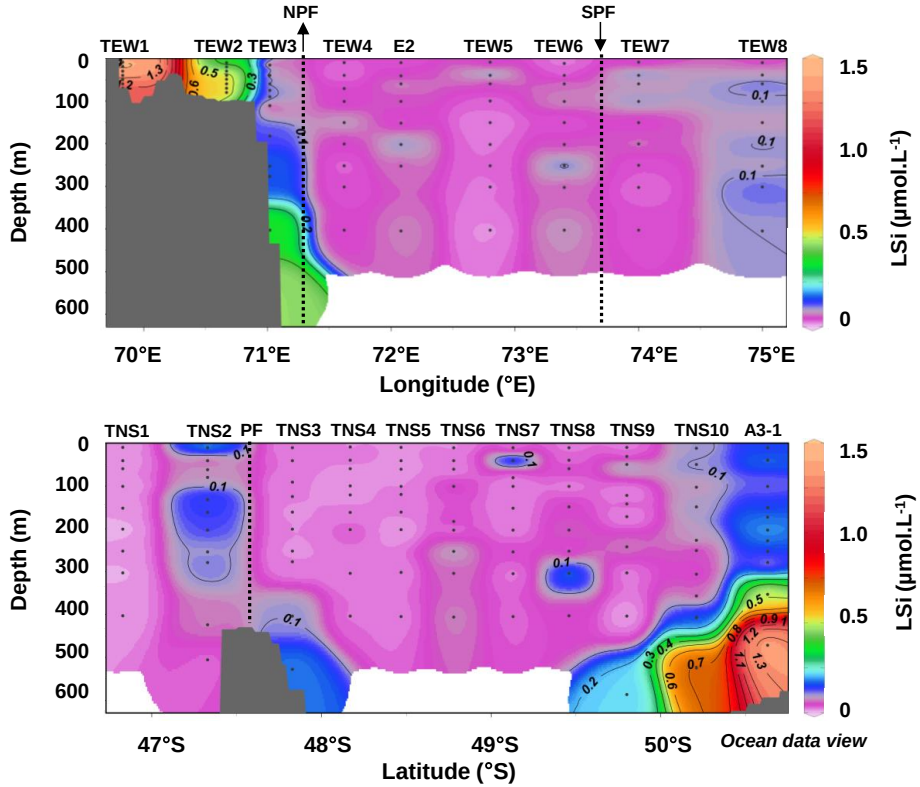

Figure 14. Vertical distribution of lithogenic silica (LSi) concentrations along the TEW and TNS transects. The dotted lines represent the approximate location of the southern branch of the Polar Front going to the North (NPF) and to the South (SPF).

BGD
11, 8259–8324, 2014

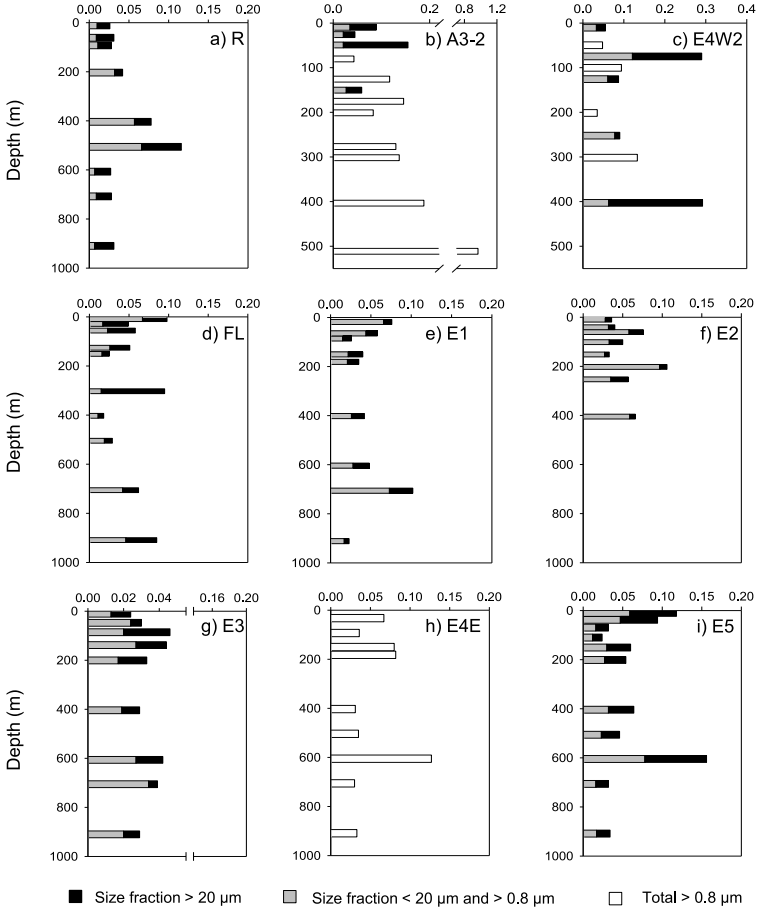

Figure 15. Vertical profiles of lithogenic silica (LSi) concentrations for three size fractions (> 0.8 µm, between 0.8 and 20 µm and > 20 µm) at stations R **(a)**, A3-2 **(b)**, E4W2 **(c)**, FL **(d)** and at stations E: E1 **(e)**, E2 **(f)**, E3 **(g)**, E4E **(h)**, E5 **(i)**.

BGD
11, 8259–8324, 2014